Geothermics 102 (2022) 102398

Contents lists available at ScienceDirect

Geothermics

journal homepage: www.elsevier.com/locate/geothermics

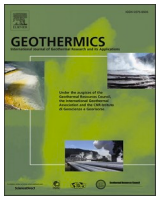

Analysis of a basement fault zone with geothermal potential in the Southern North Sea

Tiago M. Alves [a,*], Nathalia H. Mattos [a], Sarah Newnes [a], Sinéad Goodall [b]

[a] 3D Seismic Laboratory – School of Earth and Environmental Sciences, Cardiff University – Main Building, Park Place, Cardiff CF10 3AT, United Kingdom
[b] School of Chemistry, Cardiff University – Main Building, Park Place, Cardiff CF10 3AT, United Kingdom

ARTICLE INFO

Keywords:
Northwest Europe
Paleozoic
Fault zones
Heat flow
Fluid flow
Geothermal energy

ABSTRACT

Extraordinary 3D seismic data from the Central Offshore Platform (Southern North Sea), complemented by information from 38 boreholes, reveal a 10 km-wide basement fault zone above which fluid anomalies emanate from sub-salt reservoirs to terminate in lower Cretaceous strata. Fluid blow-out pipes, chimneys and low-amplitude trails were mostly sourced from the region where NW-striking syn-rift faults intersect the N-striking basement fault zone. As a result, 73% of the mapped fluid-flow anomalies (94 out of 129) occur within the basement fault zone of interest or follow a N-S strike along its shoulders. We postulate a strong control of the basement fault zone on past fluid and heat flow, as basin models confirm that fluid and heat were mostly produced during the Cretaceous. Bottom-hole data record temperatures of ~140 °C at present, highlighting the geothermal potential of the study area. These temperatures nevertheless contrast with the relatively constant gradient of ~ 32 °C/km occurring both in and outside the basement fault zone. This work is important as its shows that past fluid and heat flow over a basement fault zone does not necessarily correlate with the existence of an enhanced hydrothermal system at present. However, as bottom-hole temperatures are within the benchmark values considered across Europe, it also stresses the importance of basement fault zones as key structures to find, and assess, as potential geothermal sites.

1. Introduction

Extensional basins are considered to be favourable geological settings for the production of geothermal energy (Hurter and Schellschmidt, 2002; Omodeo-Salé et al., 2020). Fault zones in these basins, and crossing their basement rocks, can form large conduits for fluid and heat (Rowland and Sibson, 2004; Leroy et al., 2010; Arsenikos et al., 2018), as demonstrated by the Soultz-sous-Forêts and the Landau projects in the Rhine Graben, or the fault zone drilled in the United Downs project of Cornwall, United Kingdom, to cite a few examples (Kushnir et al., 2018; Vidal and Genter, 2018; Glaas et al., 2021; Reinecker et al., 2021). Fault zones can also alter the thermal evolution of sedimentary basins, which will be potentially exposed to greater heat flows close to the largest and deepest faults (Taillefer et al., 2017; Townend et al., 2017; Sutherland et al., 2017). Finally, fault zones are able to focus mineralisation and diagenetic phenomena when reactivated during discrete tectonic phases (Hooker et al., 2015; Gartman and Hein, 2019; Gomez-Rivas et al., 2019; Jiang et al., 2019). For instance, lithium concentrations in geothermal fluid of the Upper Rhine Graben have been considered high enough to justify their future economic exploitation (Glaas et al., 2021).

Basement structures tend to form dominant, regional-scale faults in terms of their size, relative displacement and influence on surrounding structures (Deng et al., 2017); in fact, large-scale normal faults often nucleate around basement weakness zones (Fossen et al., 2016; Fazlikhani et al., 2017). Despite this, both the development and growth of most extensional faults are hard to relate to specific basement structures because: (a) of the polyphasic tectonic evolution that is typically experienced by basement terrains, and (b) the occurrence of thick sedimentary (and magmatic) sequences above them, which hinder a more detailed imaging of pre-rift crustal architecture (e.g Ballèvre et al., 2018.; Festa et al., 2020; Ye et al., 2020). Difficulties in discerning inherited from younger structures are further compounded when considering different types of inheritance such as previous orthogonal rift faults affecting a sedimentary basin (Wolfenden et al., 2004), or the development of an oblique-rifting configuration dominated by specific far-field stresses and localised crustal weaknesses (Bellahsen et al., 2006). In practice, structural inheritance is more readily apparent when dealing with strike-slip and compressional settings, particularly when

* Corresponding author.
E-mail address: alvest@cardiff.ac.uk (T.M. Alves).

https://doi.org/10.1016/j.geothermics.2022.102398
Received 5 December 2021; Received in revised form 3 March 2022; Accepted 5 March 2022
Available online 14 March 2022

considering basin-bounding faults associated with large-scale orogenic processes (e.g Selander et al., 2012.; Bader, 2018). It is still not straightforward to determine how (and if) faults generated in rift settings are controlled by basement features (e.g., Finch and Gawthorpe, 2017; Festa et al., 2020).

A high-quality three-dimensional (3D) seismic volume from the Southern North Sea is used in this work to investigate a complex network of normal faults, and associated fluid flow features, along a major basement fault zone separating the Central Offshore Platform from the Broad Fourteens Basin (Fig. 1a). Seismic data reveal abundant fluid flow features above, and on the shoulders of, the basement fault of interest, a character suggesting it comprises a crustal-scale zone of weakness through which heat, gas, and other fluid is, and was in the past, able to migrate. This basement fault zone is intersected by NW-striking rift-related faults and appears not to control the nucleation of these latter structures, which kept their trends across the study area (Fig. 1b). In summary, this paper addresses the following research questions:

(1) When, in their multiple evolution stages, can basement faults zones concentrate heat and fluid sourced from deeper parts of the crust?
(2) What is the 3D geometry of basement fault zones in extensional basins as the North Sea?
(3) Are all major basement fault zones present-day sources of heat and fluid in older extensional terrains of NW Europe?

Northern Europe, in which the study area is located, has been experiencing a revival in exploration due to its volumes of unexploited natural gas, recognised geothermal resources, and preferential location for CO_2 storage (Doornenbal et al., 2019; Peuchen et al., 2019; Mulrooney et al., 2020; Wu et al., 2021; Michie et al., 2021). Many of the areas posed to produce geothermal energy in Northern Europe are associated with crustal structures that are (or were in the past) capable of focusing heat and fluid into adjacent geological reservoirs (Daniilidis and Herber, 2017; Geluk et al., 2018; Gluyas et al., 2018). They also occur over paleozoic and Mesozoic magmatic bodies (Bonté et al., 2020). Furthermore, hydrogen production and storage from gas fields has been recently equated for the North Sea in conjunction with the use of wind and other renewable energy sources (Gondal, 2019; Peters et al., 2020; McKenna et al., 2021; Scafidi et al., 2021).

2. Data and methods

This work follows a four-step method to characterise basement fault zones, as summarised below:

(1) Seismic-stratigraphic interpretations are completed in a first stage, together with the recognition of any fluid-flow features. Basement structures are mapped in detail, giving emphasis to faults and other structures that may control fluid and heat flow. The interpretation is tied to borehole data with the aim of compiling a robust seismic-stratigraphic framework to assist thermal and subsidence modelling in subsequent steps (Figs. 2 and 3).
(2) In a second stage, detailed maps of fluid and heat-flow features allow the interpreters to correlate the position and size of these features with any underlying basement structures (Fig. 2). This stage also includes the detailed mapping of fluid pipes, fluid chimneys and any other Direct Hydrocarbon Indicators (DHIs), all of which may occur at variable depths in association with the basement fault zones of interest.
(3) Stage 3 includes the analysis of fault leakage via Slip Tendency and Leakage Factor calculations. The use of regional stress data in this step is balanced against considering local stresses as predominant in a certain area (Fig. 2).
(4) In the final stage, subsidence and thermal models are used to identify if the geological conditions in a basement fault structure are favourable to the generation of heat, or to the escape of gas (either 'wet' or 'dry' gas). Bottom-hole temperatures and geothermal gradients are analysed in this stage to confirm the geothermal potential of a given prospect (Fig. 2).

2.1. Seismic and borehole data

Seismic data in this work are zero-phased with a dominant frequency of ~40 Hz. The bin spacing of the data is 25 × 25 m, while its sampling interval is 4 ms. The seismic volume was acquired in the late 2000s by the JDA partners (coordinated by NAM) and processed to reveal the structure of sub-salt gas reservoirs. All 38 boreholes drilled in the area covered by the seismic volume were tied to the interpreted seismic data

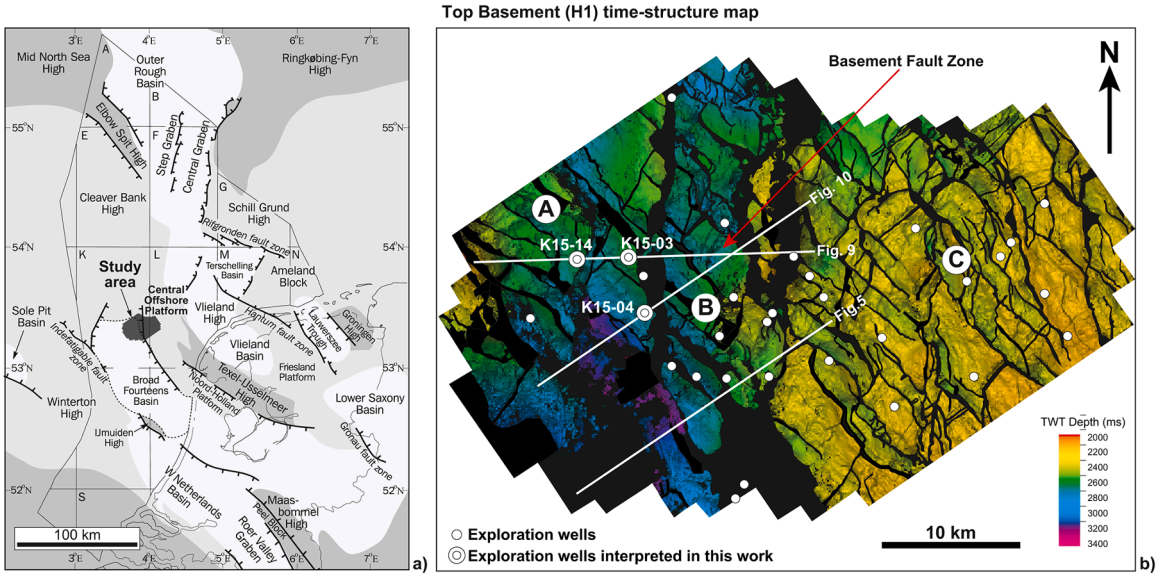

Fig. 1. a. Location of the study area, at the western limit of the Central Offshore Platform, Southern North Sea (modified from Verweij and Simmelink, 2002). (b) Structural map of the basement (Horizon H1) highlighting the basement fault zone interpreted in this work. Structural Sectors A to C are shown in the figure, with the latter zone comprising part of the Central Offshore Platform. The location of industry boreholes and seismic profiles included in this paper is also shown.

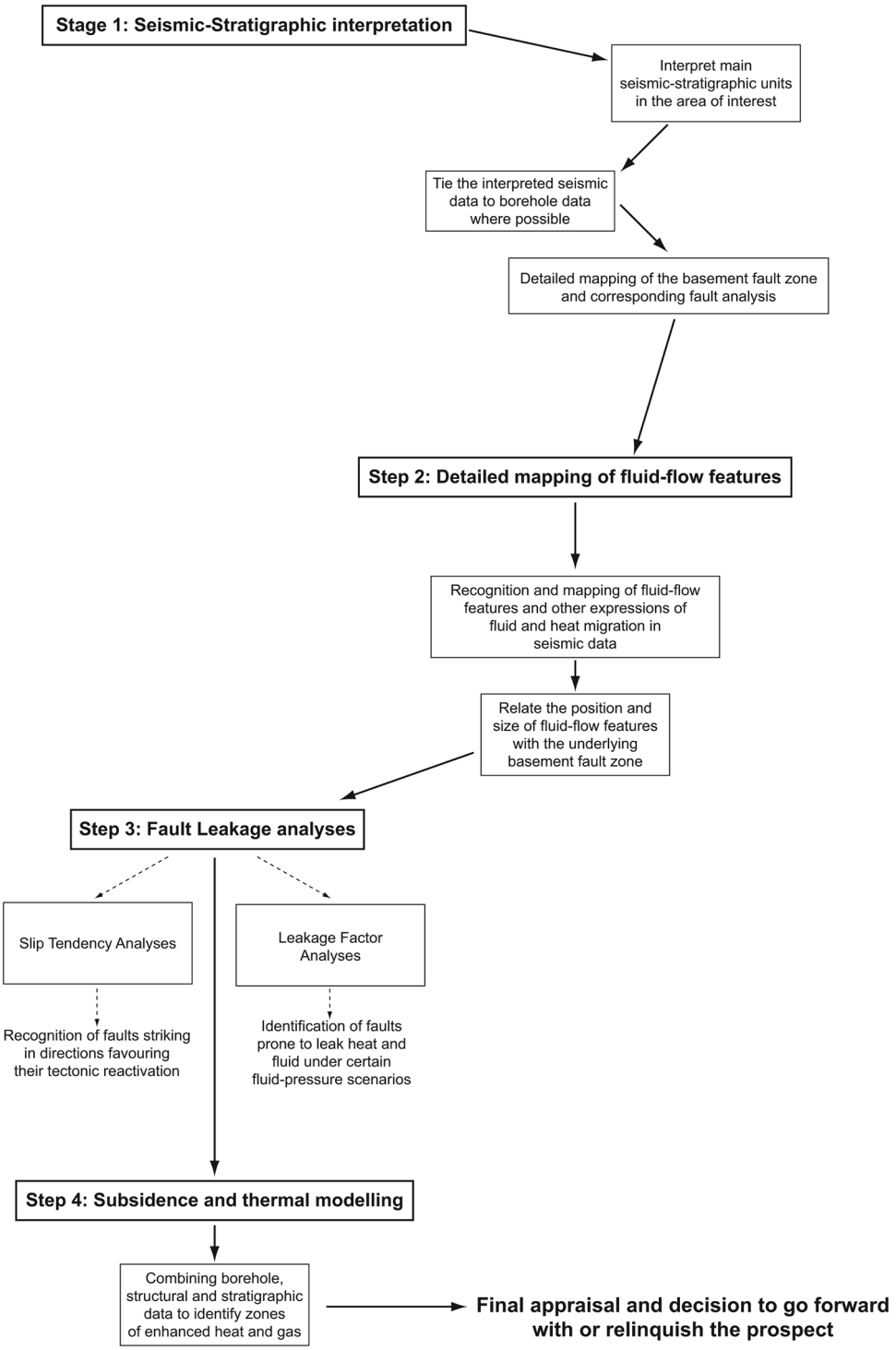

Fig. 2. Workflow suggested in this paper to assess the geothermal potential of basement fault zones.

(Figs. 1b and 3).

P-wave velocity (V_p) curves and corresponding checkshot data were gathered with their borehole completion reports from nlog.nl. When both stratigraphic and V_p data are tied to discrete seismic reflections, they reveal minimum resolutions ($\lambda/4$) of ~40 m at the depth of investigated faults, and ~20 m at the level of fluid flow features. Some of the features imaged in the basement fault zone of interest may be ~15–20 m thick in the areas where the survey has better quality, as once again demonstrated visually when correlating borehole with seismic data. Such a value approaches the maximum resolution ($\lambda/30$) expected by the interpreted seismic volume (Chopra et al., 2006; Tao and Alves, 2017; 2019).

Of the 38 interpreted boreholes, wells K15–03, K15–04 and K15–14 crossed Cenozoic and Mesozoic strata to reach paleozoic basement units (Figs. 1b and 3). They also drilled intervals in which fluid-flow anomalies are observed in seismic data. The three latter wells were used to tie our seismic data with regional stratigraphic units, and to compute thermal models using PetroMod®. Bottom-hole temperatures were also compiled and analysed, as shown in Supplementary File 1.

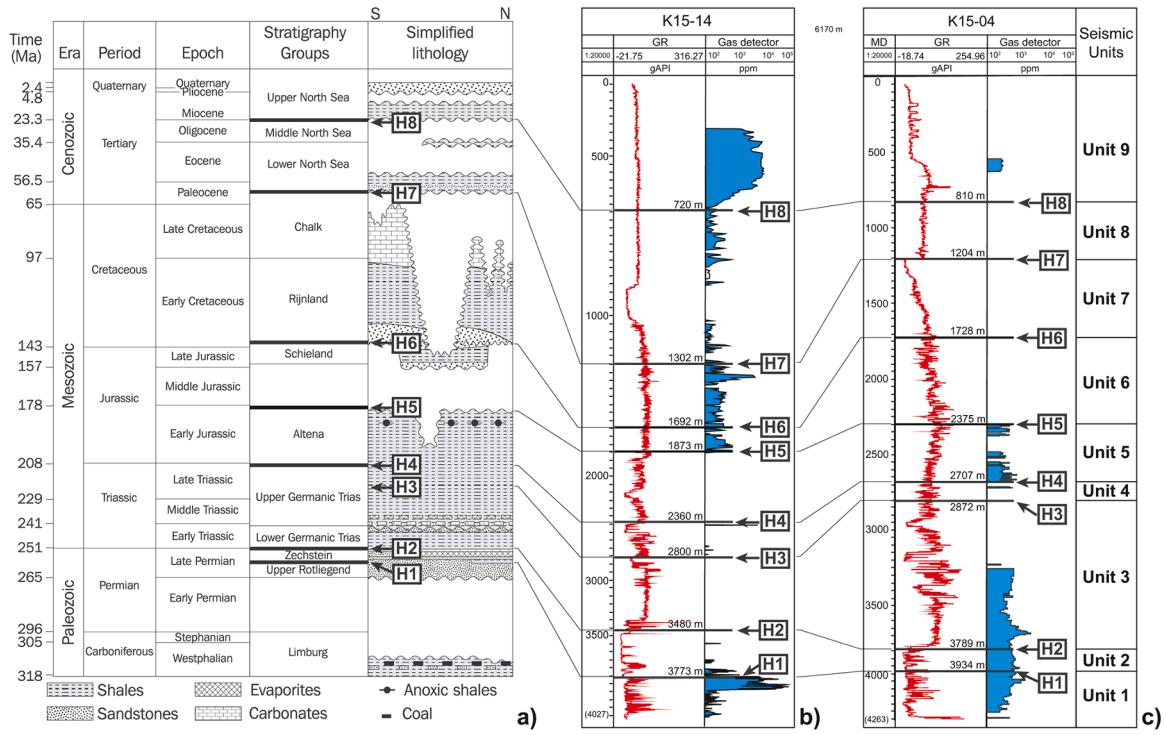

Fig. 3. (a) Stratigraphic column of the Broad Fourteens Basin correlated with the depth of seismic reflections crossed by wells K15–14 and K15–04 and a simplified lithology corresponding to each stratigraphic group in the study area. (b) Gamma Ray and Gas Detector logs for Well K15–14 showing a correlation of these two parameters along the borehole. For this well, gas was detected mainly below horizon H1, corresponding to the top of the Upper Rotliegend Group and above the base Miocene horizon H7. A smaller amount of gas is also concentrated at the Middle-Late Jurassic interval. Fluid-flow features are mostly concentrated close to the faults mapped on Figs. 1b and 5a. c) Gamma Ray and Gas Detector logs for Well K15–04 showing that a correlation between these two parameters cannot be established for this borehole. Most of the gas in this well is concentrated in the Late Permian – Middle Triassic interval. Fluid-flow features are mostly concentrated close to the faults mapped on Figs. 1b and 5a.

2.2. Structural analyses

A total of 317 basement faults were mapped every inline (12.5 m), and every five crosslines (62.5 m). Fault throws were depth-converted and measured at a pre-defined cut-off horizon (Top Rotliegend Group, Fig. 3). The faults and horizons interpreted in Petrel were then imported into Petroleum Experts' Move® as 3D mesh surfaces. For the purposes of this research, a fault family was defined as faults striking in the same direction within ±10°. Stress Tendency and Leakage Factor analyses were performed to assess the impact of past and modern stress tensors on fluid flow using the Stress Analysis Module in Move®.

Slip Tendency (T_s) reflects the likelihood of a fault to slip and is a function of the ratio of shear (τ) to normal (σ_n') stresses acting on a fault plane (Morris et al., 1996). Slip Tendency is mathematically written as:

$$T_s = \tau / \sigma_n' \quad (1)$$

Slip Tendency will vary depending on the orientation of a fault surface and the stress field acting on it. A fault will also tend to slip depending on the cohesive strength of its surface, and the coefficient of static friction (μ). On a cohesionless fault surface, slip will occur when the resolved shear stress is equal or exceeds the frictional resistance to sliding (F):

$$F \leq \tau = \mu \sigma_n' \quad (2)$$

The relative fluid transmissibility of the interpreted faults was estimated using Leakage Factor (Eq. (3)). This parameter is related to Slip Tendency (Morris et al., 1996) and defined as the ratio of pore fluid pressure (P_f) to the difference between normal (σ_n) and shear stresses (τ) on a particular fault surface. Estimated values of Leakage Factor determine the likelihood of fault-seal failure; the higher the value, the greater the likelihood of a fault to act as a pathway for fluid. Pore fluid pressures were calculated automatically in Move® by taking into account the local vertical stress, a function of the palaeo-depth of the faulted basement units, the density of strata above the basement fault zone, and the water column above the sea floor (Zoback, 2010). Similar estimates of P_f were performed taking into account the present-day stress conditions (Heidbach et al., 2016). As such, the Leakage Factor is represented as:

$$L = P_f / (\sigma'_n - \tau) \quad (3)$$

Present-day stress tensors obtained from Heidbach et al. (2016) show a prominent NNW-SSE direction of compression in the study area. In order to estimate palaeostress tensors for the Early Jurassic-Early Cretaceous syn-rift, the inversion method of McFarland et al. (2012) was applied. The fitting of the inverted stress tensors depends on a positive relationship between the Slip Tendency and displacement by assuming that fault surfaces with high Slip Tendency and large displacements relate to an early onset of slipping, whereas small fault displacements account for a later slip (McFarland et al., 2012). The magnitudes and azimuths from present-day and palaeo-regional stress tensors were considered against fluid pressure (P_f) values of 15.2 MPa during Early Jurassic-Early Cretaceous continental rifting, when the basement fault zone was at an average depth of 1375 m, and 41.4 MPa for present-day conditions, with the basement fault zone at an average depth of 3950 m (Supplementary File 2).

3. Geological setting

3.1. Geotectonic evolution

The study area is part of the Joint Development Area (JDA) of the Broad Fourteens Basin, between UK and Dutch territorial waters (Fig. 1a and b). It comprises two main N-S and NW-striking fault families first

associated with the reactivation of a complex basement fabric during Mesozoic rifting, and later with transpressional and compressional tectonics during the latest Mesozoic and Cenozoic (Ziegler, 1990; Abramovitz and Thybo, 2000) (Fig. 1b). Previous research identified horst-and-graben structures at Permian level (Schroot and De Haan, 2003), with the Rotliegend Group marking the top of the faulted basement units in the study area (Figs. 1b and 3). Zechstein salt, also Permian in age, separates a pre-Zechstein succession affected by thick-skinned tectonics from Triassic-Holocene strata experiencing thin-skinned deformation (Nalpas and Brun, 1993; Stewart and Coward, 1995; Alves and Elliott, 2014).

3.1.1. Paleozoic evolution: Caledonian and Variscan orogenies

Pre-Cambrian basement units in Northwest Europe comprise crystalline rocks that were accreted during the Caledonian orogeny, a tectonic phase that ceased during the Early Devonian (Coward et al., 2003). The Caledonian orogeny generated WNW- to NW-SE faults that were also reactivated during the Late paleozoic Variscan orogeny (Abramovitz and Thybo, 1998; 2000; Nielsen et al., 2000). The NW-SE Caledonian fault trend was specifically reactivated in the latest Carboniferous-Early Permian to generate conjugate N-S to NE-SW fault families in the North Sea (Ziegler, 1990) (Fig. 4). During the Mesozoic and Cenozoic, the two fault families (Caledonian and Variscan) yet again controlled the reactivation of faults below the Zechstein salt (Oudmayer and De Jager, 1993; Doré et al., 1997).

3.1.2. Triassic-middle Jurassic: E-W extension

The Triassic was marked by widespread E-W extension (rifting) in Northwest Europe (Ziegler, 1982). Principal Triassic rift axes strike N-S and NNE-SSW and are filled by thick successions of Upper and Lower Germanic Trias (Ziegler, 1990) (Fig. 3). Multiple rift episodes ensued after the Triassic, albeit separated by intervening stages of relative tectonic quiescence.

A renewed episode of continental rifting occurred during the earliest Jurassic (Early Kimmerian tectonic phase) and led to the deposition of the Altena Group, a unit materialising the gradual deepening of the study area (Fig. 3). Below these two latter units, at Rotliegend level, E-W extension enhanced block faulting and rotation, with the Zechstein salt decoupling the early Mesozoic strata from Carboniferous-Permian basement units. Most halokinetic structures were initiated at this time (Zanella et al., 2003).

3.1.3. Late Jurassic-Early Cretaceous: NE-SW extension

Crustal extension accelerated during the Late Jurassic-Early Cretaceous in response to the onset of continental breakup between Southwest Europe (West Iberia-Bay of Biscay) and North America, in what the literature refers to as the Middle and Late Kimmerian rifting phases (Ziegler, 1988; 1990). The direction and magnitude of extension varied significantly in Northwest Europe, but was accounted for by orthogonal rifts generated in a multi-directional extending rift system (Doré et al., 1999). This resulted in the deposition of the Schieland and Rijnland Groups, two stratigraphic groups associated with marine deposition (Fig. 3).

The main direction of extension was reoriented to the NE-SW from the Late Kimmeridgian to the Early Cretaceous, after which continental rifting ended (Deckers and Van der Voet, 2018). Farther east in the North German Basin, Jurassic-Cretaceous rifting was accommodated by dextral strike-slip movements along its southern end (Ziegler, 1990; Kley and Voigt, 2008; Scheck et al., 2002a; 2008). Late Jurassic-Early Cretaceous dextral transtensional shear along NW-trending faults was common in what is now North Germany, particularly along the Elbe Fault System, over which the modern Elbe River was formed (Betz et al., 1987; Scheck et al., 2002b; 2008) (Fig. 4).

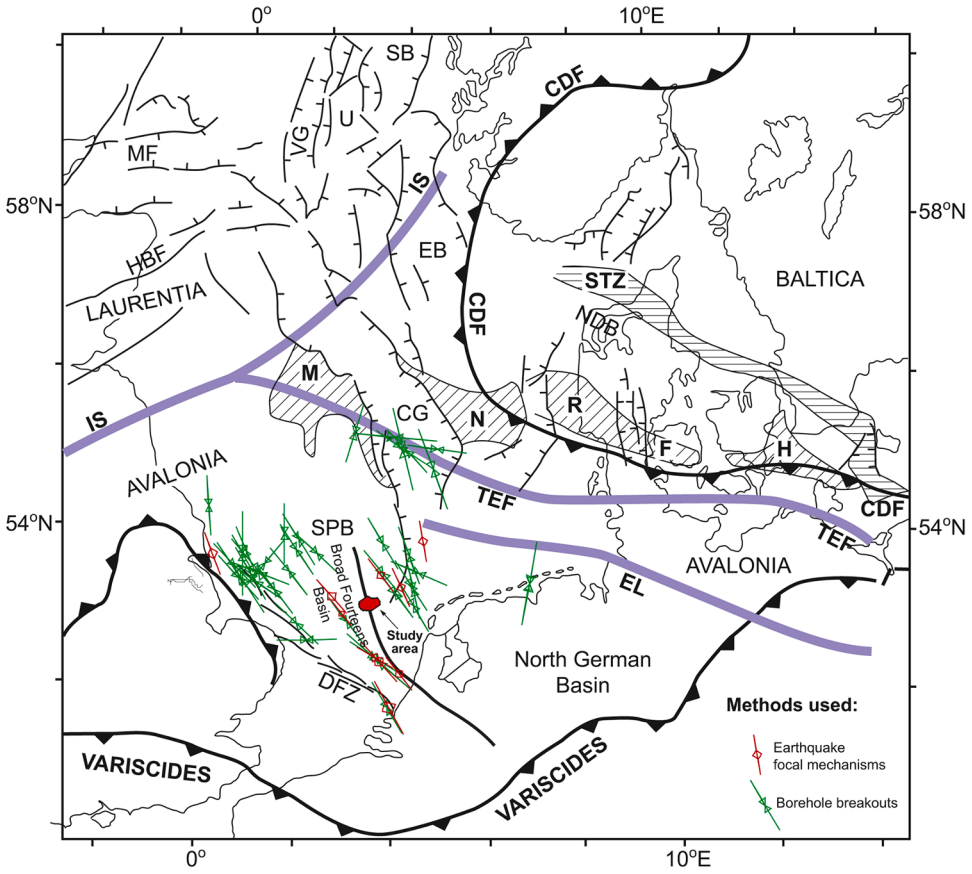

Fig. 4. Regional map depicting the main basement structures of the North Sea. Early structures at basement level were formed during the Caledonian Orogeny and resulted in the formation of a fault set trending from WNW- to NW, later reactivated in the Carboniferous-Late Permian to generate N-S to NE-SW basement faults. Note on this figure that a large N-trending basement fault zone separates the Broad Fourteens Basin from the Central Offshore Platform in the study area. CG- Central Graben; EB – Egersund Basin; MF – Moray Firth; SB – Stord Basin; SPB – Sole Pit Basin; U – Utsira High; DFZ – Dowsing Fault Zone; HBF – Highland Boundary Fault.

3.2. Alpine tectonic reactivation and supra-salt shortening

The Late Cretaceous was marked by the end of the continental rifting stage. Regional subsidence and eustatic sea-level rise ensued and led to the deposition of the Chalk Group across the Southern North Sea (Van Wijhe, 1987) (Fig. 3). Tectonic quiescence continued until de Danian (early Paleogene) before the onset of tectonic inversion due to the collision of Africa with Europe, with subsequent formation of the Alpine fold belt (Ziegler, 1988). Consequently, thermal subsidence was interrupted in the late Danian and multiple rift basins, from the British Isles to Poland, were tectonically inverted. Upper Cretaceous Chalk and Lower Tertiary clastics were eroded and thinned as a result of tectonic uplift.

Two main phases of tectonic inversion occurred during the Late Cretaceous and Early Tertiary (Ziegler, 1988, 1990, Dronkers and Mrozek, 1991; Kley and Voigt, 2008). The first is the Sub-hercynian phase, which peaked during the Campanian. Late Jurassic and Early Cretaceous faults were reactivated and, in some cases, their movement reversed. The second inversion event is the Laramide phase, peaking during the mid to late paleocene. The West Netherlands Basin, including the Broad Fourteens Basin, experienced the greatest magnitude of inversion at this time (Nalpas et al., 1995; Verweij et al., 2003).

During the Oligocene, the Labrador Sea ceased its opening and imposed a slight change in the direction of North Atlantic opening. As a result, local inversion structures were formed in the Southern North Sea during the deposition of the Lower and Mid North Sea Groups (Doré et al., 1999) (Fig. 2). The Pyrenean episode at the end of the Eocene, in particular, resulted in the tectonic uplift of the West and Central Netherland basins. Regional subsidence predominated once again after the above-mentioned episodes of tectonic inversion (Dronkers and Mrozek, 1991).

3.3. Present-day tectonic regime

A modern strike-slip to compressive regional stress field is inferred for the study area based on a variety of stress indicators (Heidbach et al., 2016). The horizontal component of maximum compressive stress is directed NW-SE, with an average azimuth of 140° (Klein and Barr, 1986). The World Stress Map (Heidbach et al., 2016) points out to a maximum horizontal compressive stress with an average N131 azimuth (Fig. 3). Such a stress tensor replicates the tectonic shortening experienced by the study area during the Cenozoic, although with a smaller magnitude when compared to the main episodes of Alpine compression.

Not all in situ stress data for the North Sea are available on the World Stress Map. Nevertheless, studies by Hillis and Nelson (2005) and Grollimund et al. (2001) highlight the notable differences that occur amongst in-situ stresses in the Northern, Central and Southern North Seas. Precise stress orientation data from drilling-induced tensile fractures show that the orientation of the maximum horizontal compression is approximately NNW-SSE in the Central and Southern North Seas, i.e., south of 58° N (Fig. 3). This orientation contrasts with the S_H value calculated by Roth and Fleckenstein (2001), in which breakout orientations below the Zechstein salt reveal a N to NE orientation at 10 locations along the NE-German basin from Berlin to the Baltic Sea, and from the Polish border to the former border between East and West Germany. Roth and Fleckenstein (2001) considered this stress rotation - from NNW to NE along northern Europe - to represent the continuation of a sub-salt structural trend already found in the NW German basin.

4. Analysis of basement structures

4.1. Stage 1 - Seismic-stratigraphic interpretation and identification of basement structures

The seismic-stratigraphy of the Broad Fourteens Basin is summarised in Fig. 3. Nine seismic units separated by eight regional unconformities were identified in the study area, with wells K15–03, K15–04, and K15–14 providing key lithological information as they drilled the basement fault zone of interest (Figs. 1b and 3). A summary of seismic-stratigraphic units and their internal character is given in Table 1.

Fig. 6a and b show, respectively, a two-way time (twt) structural map and an interpretation of main structures below the Zechstein salt. Rift-related faults are imaged as NW- to NNW-trending families that contrast with the N-S basement fault zone at the centre of the map (Sector B; Fig. 5a). This basement fault zone forms a 10 km-wide corridor from which fluid pipes and chimneys stem out and is distinct from the NW-trending Broad Fourteens Basin (Fig. 6). It separates the Broad Fourteens Basin from the Central Offshore Platform (cf Kombrik et al., 2012.) to the east (Fig. 1a).

Normal faults in supra-salt strata form intricate conjugate sets with sparse evidence for shortening (Figs. 5 and 6). In fact, Alpine tectonics is mostly documented at supra-salt level in the form of regional folding and widespread reactivation (shortening and growth) of diapirs and salt walls (Fig. 5). Below the Zechstein salt, the basement fault zone forms a mosaic of half-graben and graben structures, with most faults terminating at the level of horizon H1 (Figs. 5 and 6). Only a few N-trending faults continue to horizon H2, reaching the top of the Zechstein salt. Hence, there is a clear separation between the (inverted) supra-salt Mesozoic sequence and the faulted basement units, the latter only offset by normal faults that were not fully inverted by the Alpine tectonics (Figs. 5 and 6).

The detailed fault map in Fig. 6 confirms a dominant NW-SE fault direction at Rotliegend level over most of the study area, agreeing with past studies of the Southern North Sea (e.g Stewart and Coward, 1995.; Oudmayer and De Jager, 1993; Moeck et al., 2009). These faults are an imprint of the basement structures formed during the Caledonian Orogeny (Bartholomew et al., 1993; Coward et al., 2003), being decoupled in terms of their geometry and distribution from the N-S basement fault zone that dominates the surveyed area (Fig. 6). An important detail is that fault throw and length do not vary in a systematic way across basement fault zone (Fig. 7). Throws vary from 15 to 320 m (Fig. 7a and c). Length from 325 m to 4725 m with no clear distribution (Fig. 7c). Fault geometries are thus similar across the three zones considered, demonstrating no significant strain partition in the study area (Fig. 7). This is a character further discussed at the end of this paper.

4.2. Stage 2 - Mapping of fluid-flow features and direct hydrocarbon indicators (DHIs)

The spatial distribution of fluid pipes and chimneys in Zones A to C is shown in Fig. 8a and b. Fluid pipes and chimneys are sub-circular to oblate, but also coalesce at depth into large dim zones (Figs. 8–10). Most pipes and chimneys identified over the basement fault zone are not aligned, despite being clustered around N-trending faults and at their corresponding intersections with NW- and NNW-striking normal faults (Figs. 6 and 8). Fluid pipes and chimneys stem from faults breaching the Zechstein salt to form a series of dim zones, mud volcanoes and sub-vertical feeder zones to porous strata at Jurassic and Cretaceous levels (Figs. 9 and 10). Sector C does not show any fluid flow features despite the relatively thin salt observed there. The observation that most of the pipes and chimneys terminate at the base of the Chalk Group hints at a Late Mesozoic age for their formation (Fig. 5). Fluid sourced from basement rocks breached the Zechstein Group close to the largest faults and local salt welds. In parallel, secondary fluid migration was able to fill up-dip stratigraphic traps along rafts comprising Triassic and lower Jurassic strata (Alves and Elliott, 2014) (Fig. 5).

Vertical features such as pipes and dim spots are particularly abundant within and along the basement fault zone in Sector B (Fig. 8b). They appear as sub-circular features on RMS amplitude and structural maps, as shown in Fig. 8b. Approximately 73% (94 out of 129) of the mapped fluid-flow features occur or within the basement fault zone (Sector B) or

Table 1
Summary of the principal features of seismic-stratigraphic units in the JDA, Broad Fourteens Basin.

Seismic Unit	Age of base	TWTT Thickness (ms)	Internal character, geometry and terminations	Lithology	Lithostratigraphic Groups
Unit 9	Miocene	500–700	High- to moderate-amplitude sub-parallel reflections. Locally eroded by channels. N-dipping clinoforms.	Clay and fine-grained to coarse sand, locally gravel or peat and brown-coal seams.	Upper North Sea Group
Unit 8	middle Paleocene	400–1000	Low- to moderate-amplitude internal reflections, tightly faulted. Most faults are polygonal in map view. Local growth is observed near growing salt structures.	Sands, silts and clays of a predominantly marine origin.	Middle and Lower North Sea Group
Unit 7	Hauterivan	400–1000	Low- to moderate-amplitude internal reflections, with good continuity. Represented in most of the study area and covering syn-rift depocentres	White, buff, cream and light grey, hard, fine-grained, bioclastic/marly limestones. Clay and sandstone beds.	Chalk Group Rijnland Group
Unit 6	middle Callovian	0–500	High- to moderate-amplitude strata filling the upper part of bowl-shaped depocentres. Often faulted and limited in its extend and thickness.	Grey and variegated claystones, coaly to clayey sandstones, rarecoal, and calcareous intercalations.	Schieland Group
Unit 5	latest Triassic (Rhaetian)	0–1000	Low- to moderate-amplitude internal reflections. Strata grows in bowl-shaped basins delimited by salt diapirsand pillows. High-amplitude intervals denote high-TOC shales.	Fine-grained mudstones with occasional silt- and sandstones. Organic-carbon concentrations.	Altena Group
Unit 4	Middle Triassic (Ladinian?)	0–125	Moderate- to high-amplitude parallel reflections showing lateral pinch-outs onto salt structures. It forms the upper part of Triassic deposits below growing, syn-rift strata.	Variegated, silty claystones, evaporites, carbonates and sandstones.	Upper Germanic Trias Group
Unit 3	latest Permian (Changhsingian)	200–600	High- to moderate-amplitude parallel internal reflections. Forms the first strata above salt diapirs and pillows. Halokinesis tilted and faulted this unit in most of the study area.	Red-bed-type sandstones, siltstones and claystones.	Lower Germanic Trias Group
Unit 2	Late Permian (Wuchiapingian)	50–2500	Chaotic to diffractive internal reflections. High amplitude carbonate intervals ('stringers') locally imaged. Forms the core of salt diapirs and pillows.	Evaporites and carbonates with some thin intercalations of claystone.	Zechstein Group
Unit 1	Carboniferous	100–600	Moderate-amplitude, parallel internal reflections. Faulted and forming a mosaic of locally tilted strata below the Zechstein salt. Half-graben/ graben blocks are visible.	Conglomerates, claystones, sandstones predominantly of red-bed type and evaporites. Grey to black sediments with coal seams in the Limburg Gr.	Rotliegend Group Limburg Group

along its shoulders (Fig. 8b). Only 27% (a total of 35) of these fluid-flow features do not emanate from the basement fault zone, with 17 of these 35 features being associated with a salt structure in Sector A (Fig. 8b). Such a relationship is clearer if one considers that gas is chiefly sourced from the Rotliegend Group, with basement faults, chasms separating Triassic-Jurassic rafts, and faults parallel to these latter, forming the preferential structures through which this gas migrates (Figs. 8–10).

One key observation in seismic data is that the largest pipes and chimneys occur where the Zechstein salt is most deformed. In addition, the strike of chasms and listric faults in the Triassic-Jurassic rafts is mostly perpendicular to raft movement and related to the NW–SE and NNE–SSW basement structures mapped in Fig. 6. Regardless if the main sources of fluid occur at Carboniferous level or in lower-crust rocks, relatively shorter and smaller pipes are observed in the areas with the thickest salt (Figs. 9 and 10).

4.3. Stage 3 - Fault-leakage analyses

Stage 3 comprises the computation of Leakage Factors for faults in the study area (Fig. 2 and Supplementary File 2). In our models, stresses were assumed to comprise a vertical σ_v of 33 MPa and a sub-horizontal σ_3 with a N240 azimuth during Mesozoic extension (Fig. 11). For present-day conditions, a vertical σ_1 of 80 MPa and a sub-horizontal σ_3 trending N131 were estimated based on Heindbach et al. (2016) (Fig. 12).

Leakage Factors for faults crossing Upper Jurassic-Lower Cretaceous strata vary from 0.5 to 2.3 for a pore-fluid (P_f) pressure of 15.2 MPa, indicating a medium to high tendency of these faults to leak (Supplementary File 2). The average Leakage Factor for faults in the basement fault zone is ~1.1–1.2 during the Mesozoic, pointing to a significant tendency for faults to leak. Importantly, the highest leakage factors (up to 2.2) are recorded in N-striking faults in Sector B, whereas the NW-striking faults show comparatively small Leakage Factors at ~1.3 (Fig. 11).

Distinct Leakage Factors are obtained taking into account the present-day stress conditions (Fig. 12). A pore fluid pressure of 41.4 MPa was considered for this estimation (Supplementary File 2). Leakage Factors at present are similar to the Late Jurassic-Early Cretaceous, varying from 0.50 to 2.3, with faults in Sectors A to C showing an average Leakage Factor of 1.5 (Fig. 12). However, the basement fault zone (Sector B) shows relatively moderate Leakage Factors around 1.5–1.6, with the largest values being related to the intrinsic geometric complexity of the interpreted fault planes. This complexity is capable to impose local increases in Leakage Factors (Fig. 12).

In summary, Leakage Factor models using regional stress data (Heidbach et al., 2016) reveal that normal faults in the basement fault zone constitute, at present, paths for fluid sourced from basement rocks (Fig. 12). In comparison, Leakage Factors estimated for the Late Jurassic-Early Cretaceous rifting suggest a larger tendency for fluid to flow from the basement fault zone, justifying the presence of Late Mesozoic pipes and chimneys in the study area (Figs. 5 and 11).

4.4. Stage 4 - Subsidence and thermal modelling

The burial and thermal histories of the three wells considered in this work were computed using PetroMod® (Fig. 13 and Supplementary File 3). Two of the wells (K15–03 and K15–04) drilled the western shoulder of the basement fault zone of interest, where a cluster of fluid flow anomalies is observed. The third well (K15–14) is located 2.5 km to the west of the basement fault zone (Figs. 6 and 9).

Well K15–03 targeted a footwall block below the Zechstein Salt but did not find gas above this evaporite succession. The well is located in the immediate shoulder of the basement fault zone in Sector B (Fig. 6). Well K15–04 targeted Rotliegend strata below the Zechstein Salt and

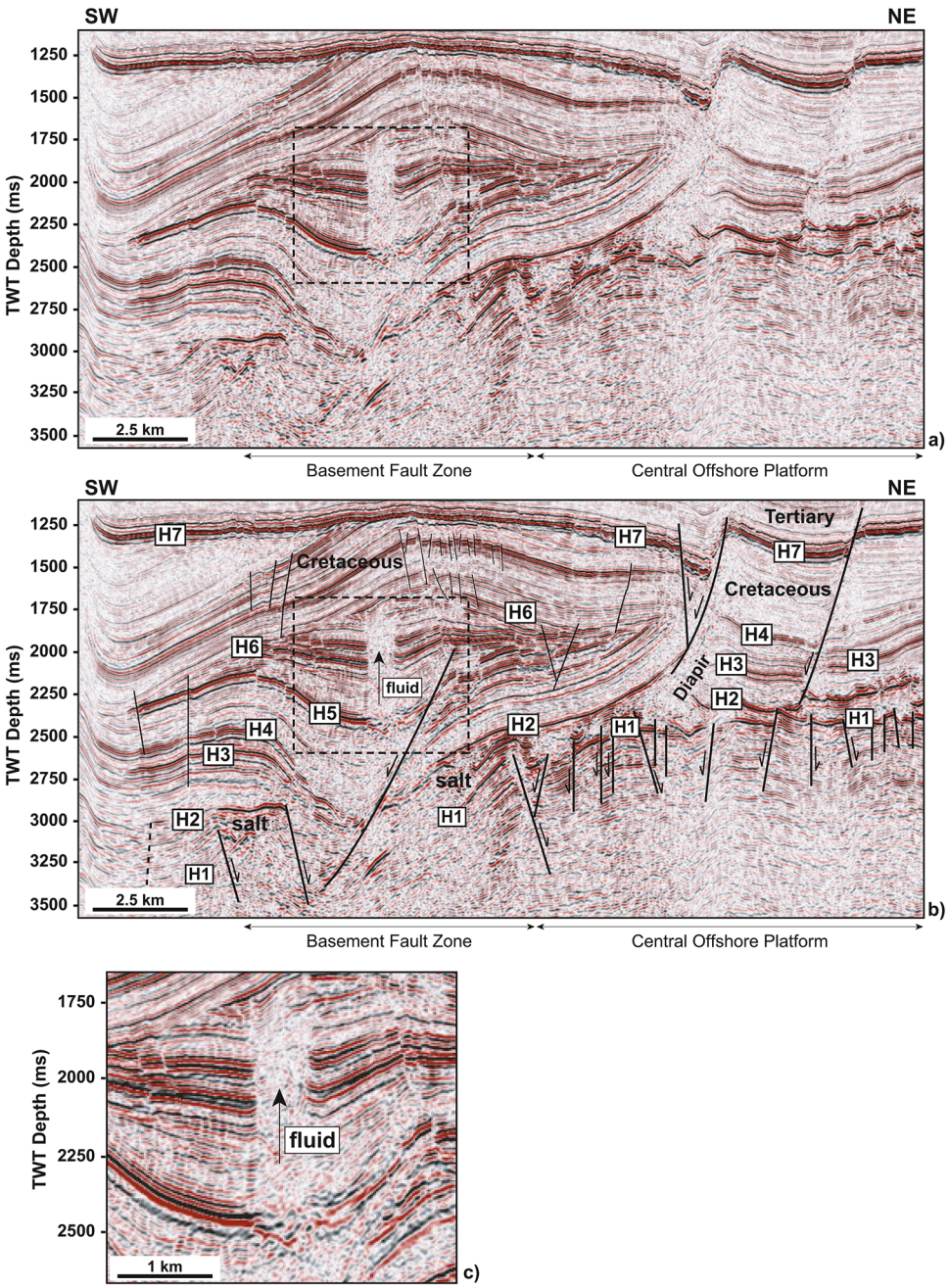

Fig. 5. (a) Uninterpreted SW–NE seismic profile showing evidence of vertical fluid flow features developed on a normal fault bounding the basement fault zone to the east. (b) Interpreted seismic section revealing main seismic stratigraphic markers and faults in the study area. See Fig. 1 for location and Fig. 2 for relative ages for key seismic-stratigraphic markers. Fluid flow features in a) and b) are observed in Mesozoic strata above the Zechstein salt and are rooted in the basement fault zone imaged in Fig. 1b. Note the change in the relative depths, spacing and fault throws within the basement fault zone, striking N-S, when compared with the Central Offshore Platform to the northeast (Sector C in Fig. 1b). (c) Zoomed-in section of the seismic profile in b) highlighting the internal character of fluid-flow features in the study area.

found evidence for the presence of gas at Jurassic and Late Cenozoic levels (Figs. 2, 5 and 6). It was drilled over a basement horst flanking the basement fault zone. Well K15–14 was drilled close to K15–03 (Fig. 6) and found abundant evidence of gas at Cenozoic and Cretaceous levels. The well is located close to fluid flow anomalies that are imaged in Mesozoic strata (Figs. 2 and 8).

All wells show that temperatures were enough to produce hydrocarbons (mainly gas) during the Early Cretaceous, when the study area was evolving under its latter (and most important) phase of continental extension. Close to the shoulder area of the basement fault zone, a second stage of subsidence is recorded during the Paleogene in wells K15–03 and K15–14, leading to a second episode of hydrocarbon maturation and, putatively, fluid migration (Fig. 13a and b). In contrast, Early Jurassic continental rifting did not result in markedly higher heat flows, as the basin was filled by relatively thin post-Zechstein sediment. Basement rocks (see Limburg Group in well K15–04) are now buried under more than 4 km of strata (Fig. 13b). Carboniferous coal has been capable of producing gas since the Early Cretaceous, with a brief hiatus in the early Paleogene in well K15–03. It is plausible to consider that gas was present at this time with enough volume to migrate along the largest faults in the study area (Fig. 13a).

5. Present-day heat and fluid flow within an offshore basement fault zone

A key piece of information is gathered from bottom-hole temperatures in Sectors A to C. Bottom-hole data record temperatures of ~140 °C at Rotliegend level, confirming the geothermal potential of the study area. However, based on the graph in Fig. 14, one can observe that Sectors A to C do no show much difference in bottom-hole temperatures and corresponding geothermal gradients. Bottom-hole temperatures correlate very well with the PetroMod® thermal modelling in Fig. 13,

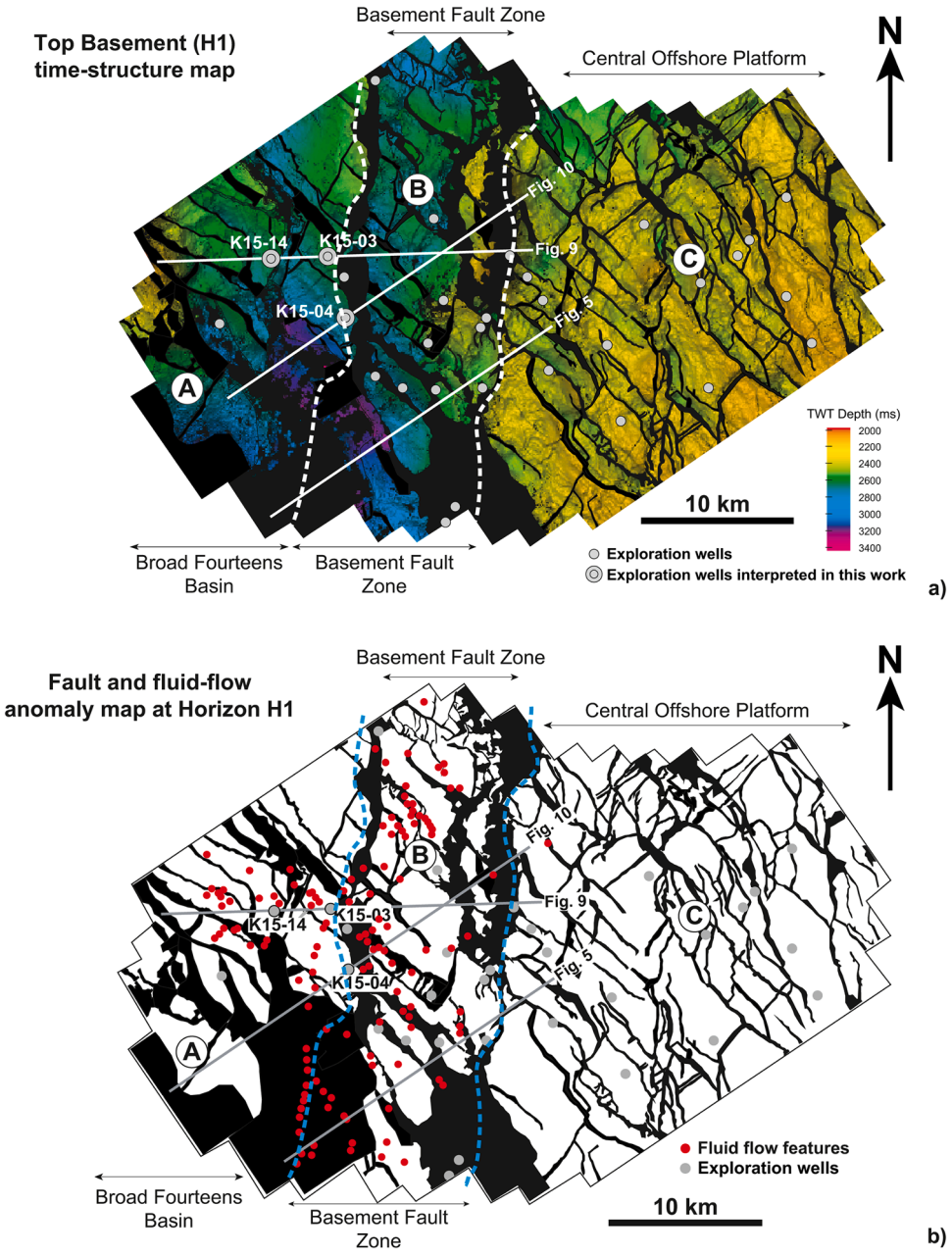

Fig. 6. (a) Structural map of the basement (Horizon H1) highlighting the basement fault zone in this work and the location of key wells. (b) Fault map resulting from the removal of the Top Basement (H1) structural map in Fig. 6a, highlighting fluid flow features (red circles) in Sectors A to C.

being only 0–15 °C hotter than the models, but also reveal that thermal gradients are now rebalanced across Sectors A to C. Sector A has the lowest geothermal gradient (30.45 °C/km), a value not dissimilar to the 31.45 °C/km recorded over the basement fault zone (Fig. 14). Interestingly, Sector C is the one recording the greatest geothermal gradient with 33.01 °C/km (Fig. 14).

Leakage Factor analyses indicate that faults in the centre of the basement fault zone, at an angle with the direction of extension, are the structures recording the largest Leakage Factors during the Mesozoic (Fig. 11). In contrast, present-day Leakage Factors indicate that those faults striking parallel to the maximum horizontal stress have the maximum potential for fluid flow (Fig. 12). There is also little variation in Leakage Factors with changing angles of dip - any surface orientated parallel to the maximum horizontal stress (± 40°) with a dip greater than ~35°, has a Leakage Factor greater than that for the perpendicular fault set (Fig. 12).

The modelling approach in this work assumed the Rotliegend Group to be the main reservoir of heat in the study area. The software used in our analysis assumes that a reservoir is isotropic and, for every MPa decrease in fluid pressure, a 1 MPa increase occurs in all principle stress orientations, or vice-versa. Since reservoirs are in reality anisotropic, the vertical stress often remains unaffected by depletion-based stress changes, or by compressional tectonic stresses, whilst horizontal stresses are usually affected (Engelder, 1993). As a result of assuming an isotropic stress distribution in our fault modelling, changes in effective vertical stress did not impact fault leakage values as expected from a typical anisotropic sandstone reservoir. Verweij et al. (2011) have shown that reservoir fluid pressures at Rotliengend level varied throughout the tectonic history of the Southern North Sea; the greatest overpressures occurring during Late Cretaceous-Early Tertiary tectonic inversion. If overpressure generation was, at this time, significant enough to exceed the retention capacity or induce hydraulic fracturing,

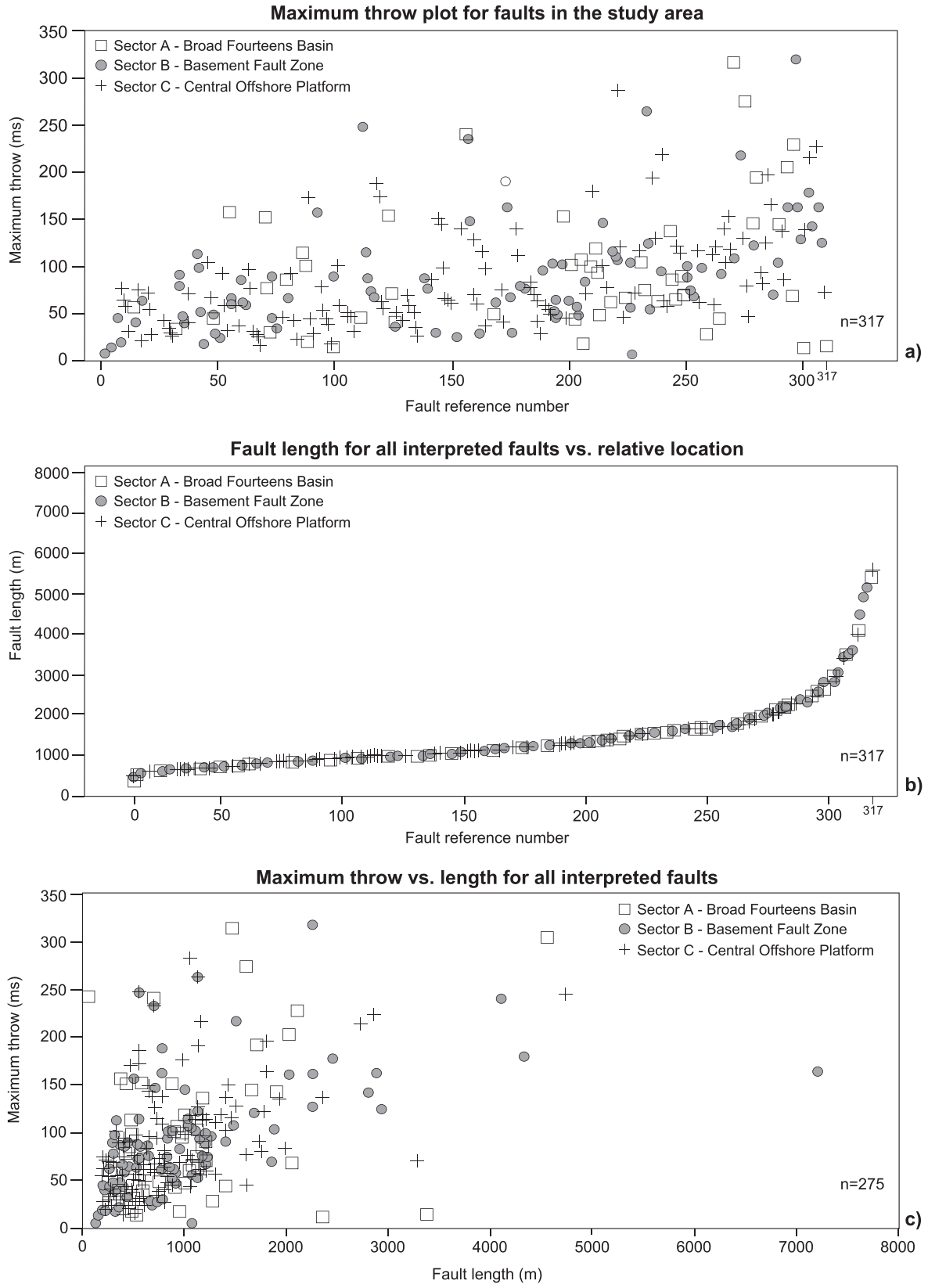

Fig. 7. (a) Maximum throw plot for the 317 faults analysed in this work. Fault throws are discriminated for the three zones (Sectors A, B and C) considered in this paper, with values forming a random cluster on the graph. The only clear trend observed is that of Sector C showing relatively low maximum throws in most of the interpreted faults. (b) Fault length plot stressing the apparent random distribution of lengths in the three sectors A, B and C, but with the larger faults comprising structures >5000 m long. (c) Maximum throw vs. length plot for the 317 faults interpreted in the study area. The random distribution of throws and lengths is clear in the graph for the three sectors considered.

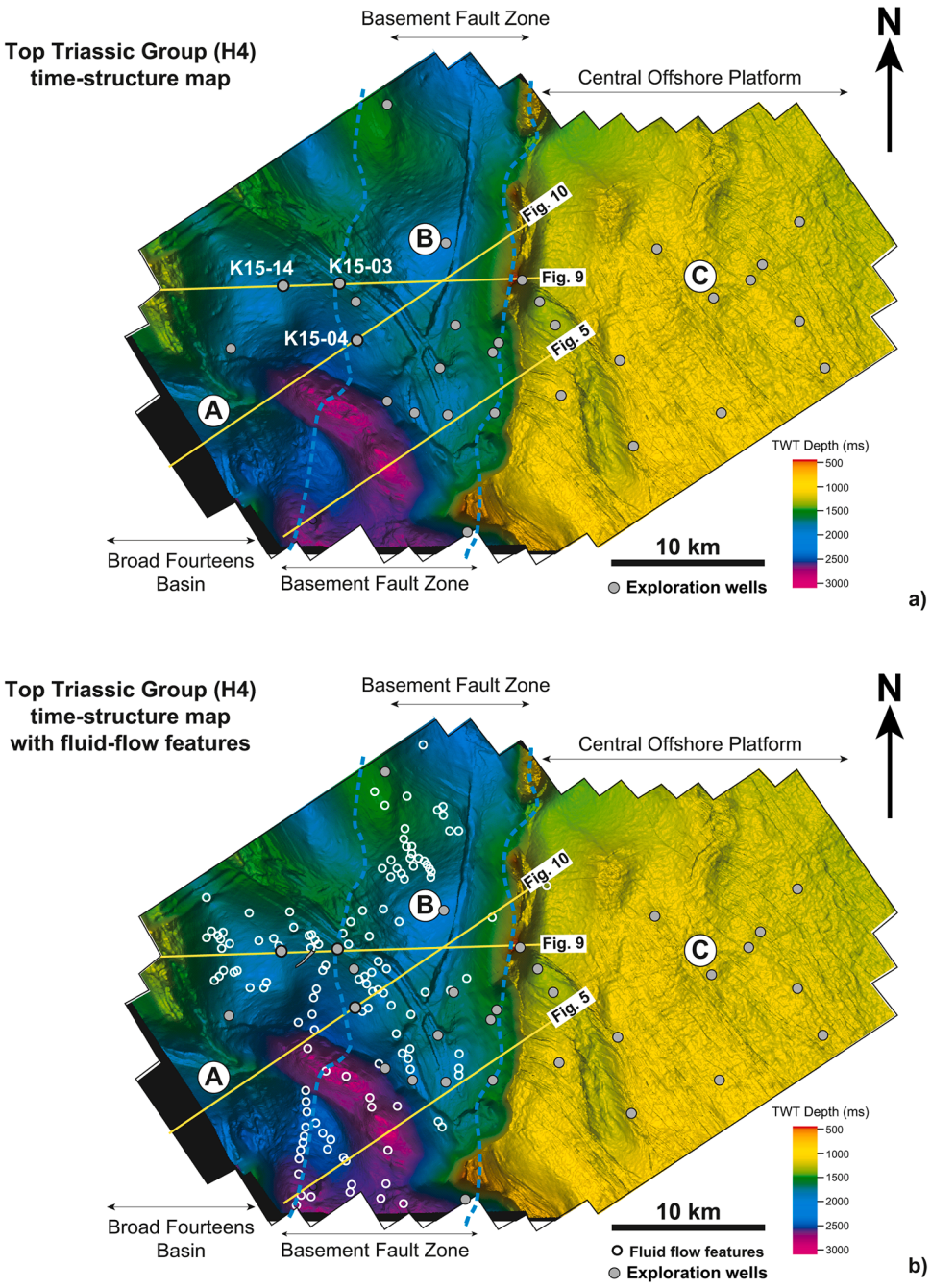

Fig. 8. Time-structural map of the Top Triassic Horizon H4 revealing the structural trends in Sectors A to C. (b) Time-structural map of the same horizons showing the location of fluid flow features, such as pipes and dim zones (white hollow circles) crossing lower Mesozoic strata.

the integrity of the Rotliegend reservoirs (and overlying traps) may have been compromised. Fluid flow in the study area is thus interpreted to have responded to the combined effect of N-S basement reactivation during the Mesozoic, the development of NW-SE rift-related faults, and subsequent Late Cretaceous-Tertiary tectonic reactivation. The fact that no preferential strain partitioning is observed along and across the basement fault zone can be explained by the reactivation of heavily compartmentalized basement units, with multiple fabric trends being reactivated in distinct directions during syn-rift.

6. Discussion

6.1. 3D geometry and evolution of a basement fault zone

Fig. 15 summarises the structural evolution of the study area. The relatively high likelihood of leakage during the syn-rift (Kimmerian) is due to the small differential stresses recorded between σ_1 and σ_3. The predicted history of vitrinite reflectance for the Westphalian Limburg coal source rock indicates that gas generation began at the end of Early Kimmerian rifting (Verweij et al., 2003; Doornenbal et al., 2019). The predicted relative high leakage along NW-SE faults during this period is therefore unlikely to have contributed to a significant loss in gas or other fluid (Fig. 15).

Present-day stress also favours fluid flow along NW-SE faults, with

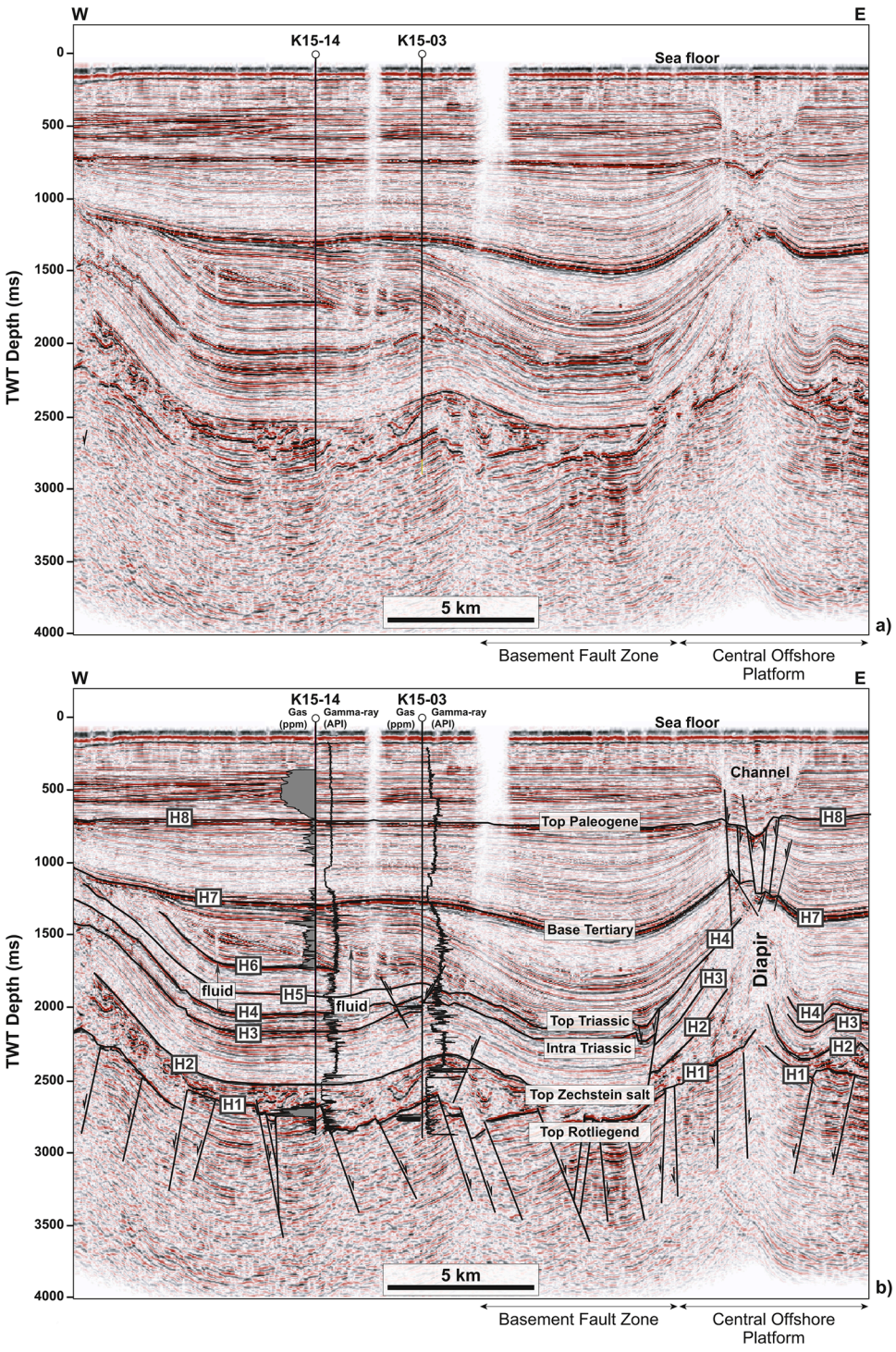

Fig. 9. (a) Uninterpreted W-E seismic profile crossing wells K15–14 and K15–03. to highlight the location of fluid pipes close to the wells and the location of the basement fault zone. (b) Interpreted W-E seismic profile crossing wells K15–14 and K15–03 denoting the stratigraphic intervals in which gas accumulations are recorded. Note the presence of the basement fault zone immediately to the east of well K15–03. Close to well K15–14, the gas pipe is small, and faults are observed only in the basement fault zone, resulting in a relatively higher accumulation of gas for this well.

maximum Leakage Factors around 0.5 and 2.3 respectively. Hence, the results in this work differ to a similar study by Moeck et al. (2009) (Fig. 15). In the North German basin, Moeck et al. (2009) defined two fault trends at Rotliegend level that are identical to those found in our study area. Based on hydraulic fracturing and pressure stability test data from numerous drill holes, the trend of the maximum horizontal stress was estimated to be N-S to NNE–SSW in the eastern part of the northeast German basin, reflecting a regional strike-slip regime. According to Moeck et al. (2009), this regime turns NW-striking faults into low-flow structures while N-striking faults become high-flow structures; high normal stresses imposed on the former structures prevent tensional failure.

The NW-SE fault families in the Southern North Sea show anomalously high length-to-throw ratios, with lengths of up to 25–30 km but maximum throws of only ~300 m (Oudmayer and De Jager, 1993). The maximum throw of ~300–350 m for the 317 faults interpreted in the study area is similar to that documented in Oudmayer and De Jager (1993). They also present a scattered range of throws and lengths (Fig. 7). Such a characteristic has been considered as reflecting the significant reactivation of fault families throughout their evolution (Kim and Sanderson, 2005).

In the study area, ESE-WNW and NNE-SSW faults are also observed,

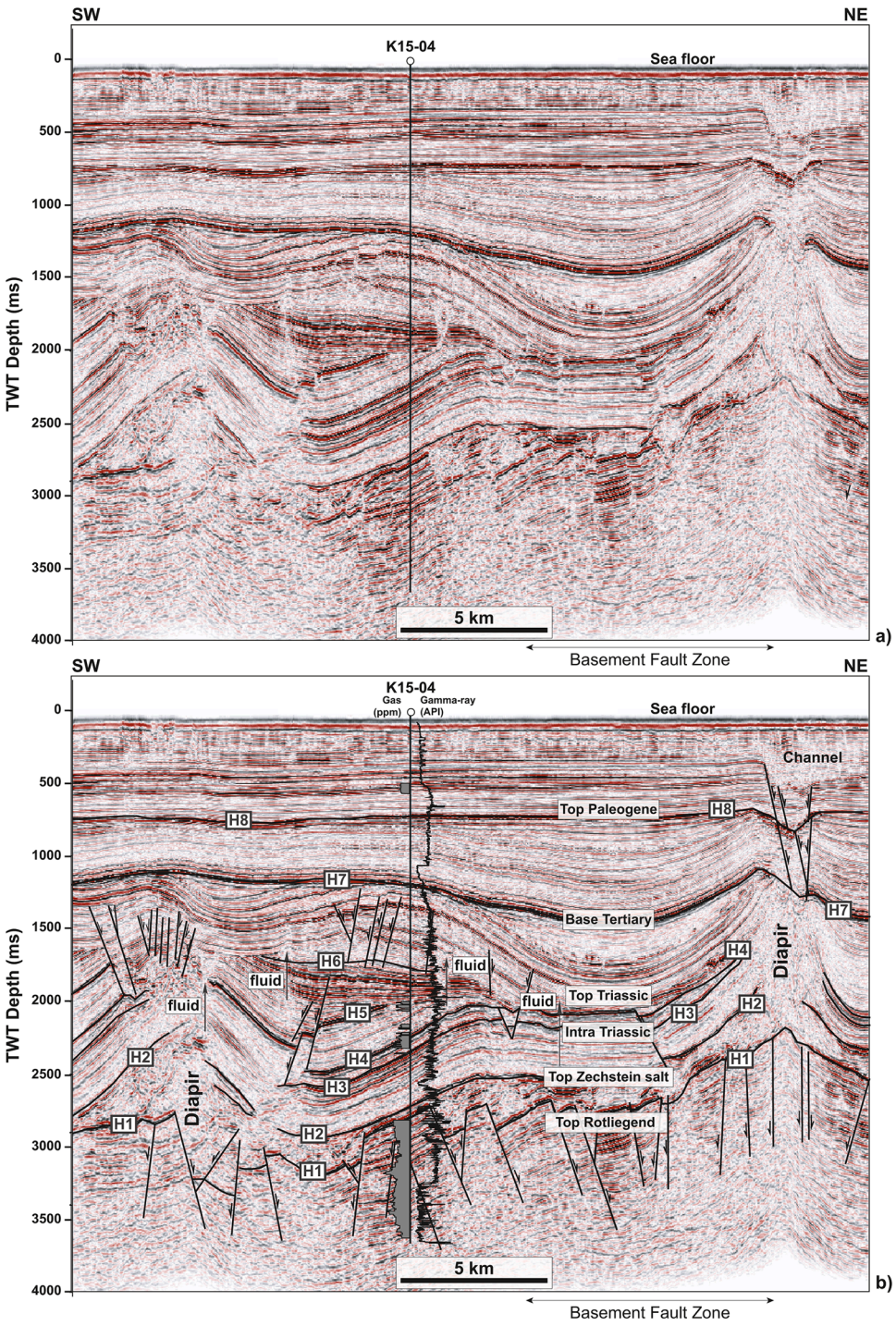

Fig. 10. (a) Uninterpreted SW-NE seismic profile crossing well K15–04 to highlight the structural complexity of this profile and indicating the location of fluid pipes close to the wells and the basement fault zone. (b) Interpreted SW-NE seismic profile crossing well K15–04 to indicate the largest accumulation of gas on the shoulders of the basement fault zone. The fault close to this well juxtaposes horizons H1 and H2, respectively equivalent to the Top Rotliegend and the Top Zechstein salt, thus revealing the salt as a competent seal. Note that gas pipes are located either at the crest of a salt diapir or close to faults.

though less commonly. They have been identified in the literature as faults formed in order to accommodate oblique-slip during multiple tectonic events (Oudmayer and De Jager, 1993). ESE-WNW faults have little expression in the supra-salt overburden - such a fault orientation is believed to have formed in response to pre-Variscan Carboniferous extension (Fraser and Gawthorpe, 1991). Conversely, the NNE-SSW fault family reflects the orientation of salt diapirs and pillows in the study area, agreeing with studies denoting a preferential distribution of halokinetic structures in this direction (e.g., Stewart and Clarke, 1999.; Zanella et al., 2003; Van Gent et al., 2010).

A question that immediately arises from this work is why are fluid pipes and chimneys preferentially located over the basement fault zone? One can first evoke that Carboniferous coal matured first around the basement fault zone, which later formed a region in which gas was preferentially fed to shallower parts of the Broad Fourteens Basin. This mechanism implies that subsidence associated with the fault zone (relative to the Central Offshore Platform) resulted in the early maturation of the Carboniferous coal, i.e. before the Late Cretaceous-Tertiary age estimated for gas generation in the study area (Verweij and Simmelink, 2002) (Figs. 6 and 8). If that is the case, gas pipes younger than the Late Cretaceous should be present in Sector C, and also through most of Sector A, as these would have been fed from coal reaching the maturation window relatively late. In contrast, these fluid flow features are located along the basement fault zone, or on its western shoulder,

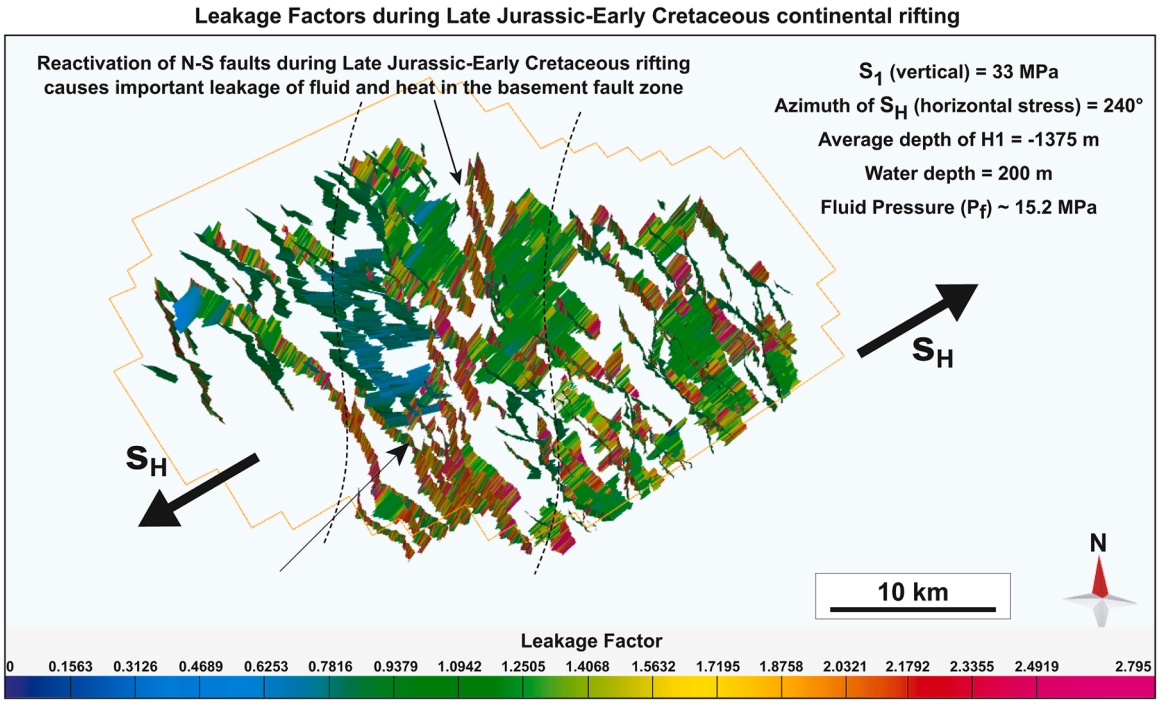

Fig. 11. Leakage Factors calculated for the basement faults during Mesozoic extension revealing high leakage factors for N-trending faults. The estimated paleo-stresses are shown in the figure and further explained in Supplementary File 2.

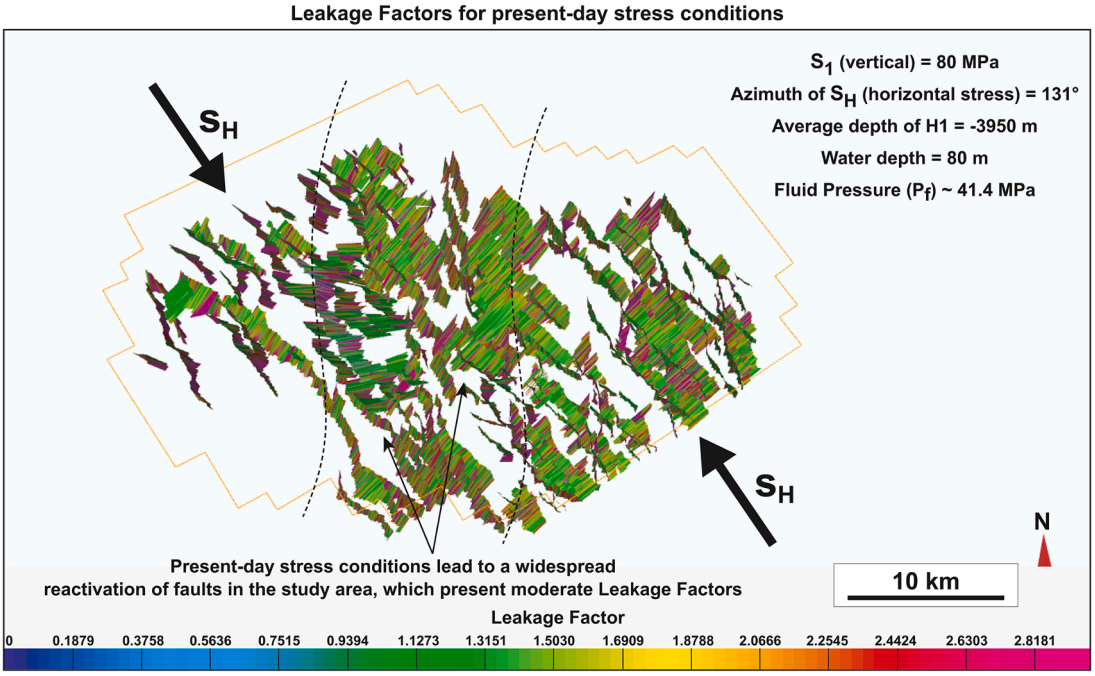

Fig. 12. Leakage Factors calculated for the basement faults considering the present-day stress conditions, a profile depth of −3600 m (estimated from the seismic data), and a pore-fluid pressure of 41.4 MPa. For these faults, Leakage Factors are smaller than during the Early Jurassic – Early Cretaceous continental rifting. Present-day stresses were obtained from Heidbach et al. (2016).

despite the fact that Sectors A and C comprise multiple gas fields at sub-salt level (Fig. 8).

A second hypothesis considers enhanced fluid flow from the Mesozoic to the present-day (Fig. 15). A putative fault-related conduit for fluid and heat reaching as deep as the lower crust must be equated in this case. In such a setting, the apparent rooting of pipes around and inside the basement fault zone, despite this being the area of thicker Zechstein salt, is explained by fluid reaching a critical stress below the salt, with pipes breaching it when vertical (σ_v) and capillary pressures in the salt are reduced or salt is breached by propagating basement faults (Fig. 15). However, bottom-hole temperatures for Sectors A to C do not indicate any major differences, rebuking this hypothesis. Instead, there is evidence in this work for a rebalancing of Late Mesozoic heat flow across the study area, with no major differences in Sectors A to C at present.

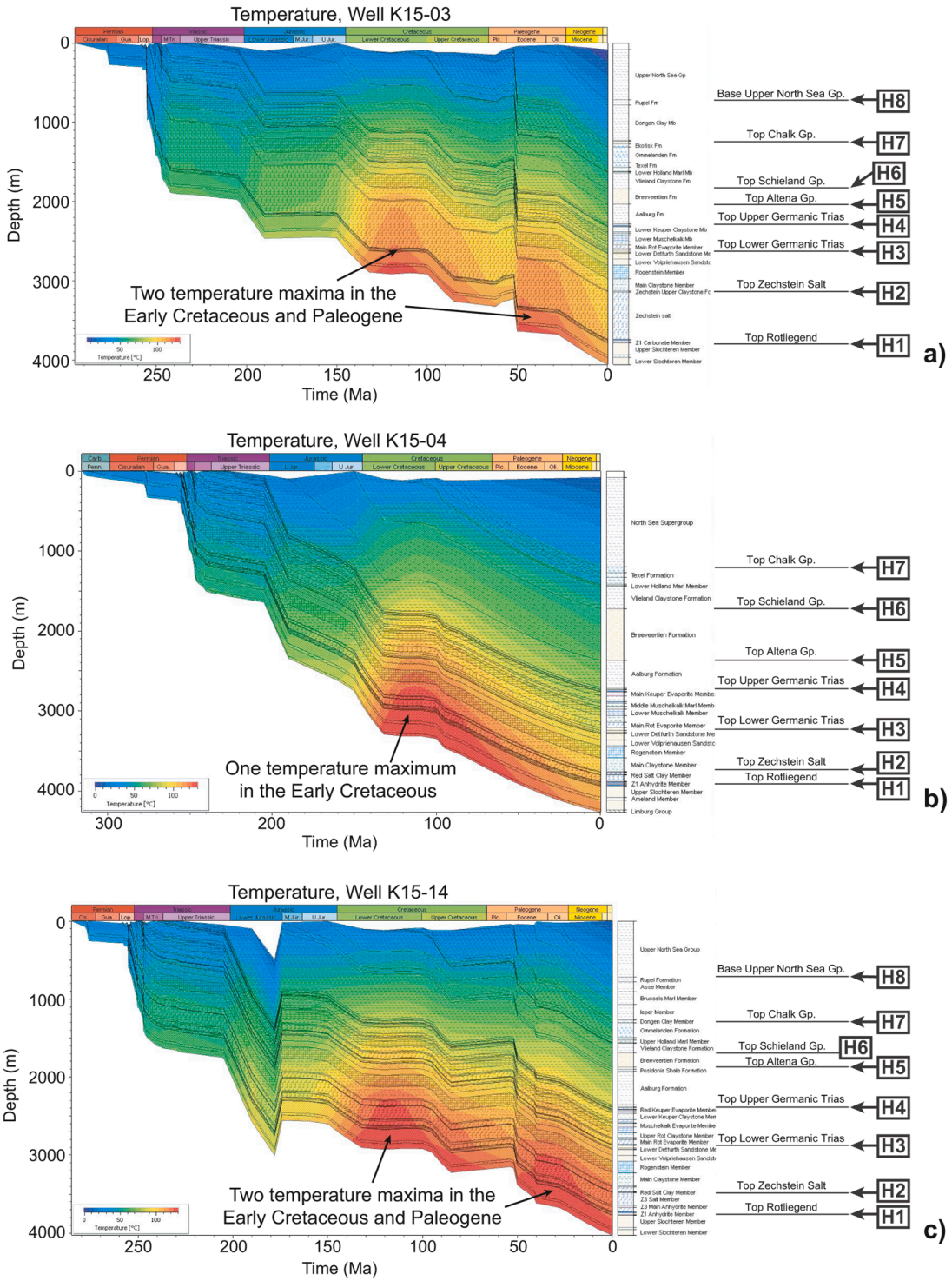

Fig. 13. Subsidence and thermal models for wells (a) K15–03, (b) K15–04 and (c) K15–14, located within the Basement Fault Zone. The subsidence and thermal models provide evidence for multiple phases of maturation in Rotliegend and older strata near the basement fault zone. Wells K15–03 and K15–14 reveal Early Cretaceous and late Paleogene increases in temperature and subsidence during major tectonic events.

As suggested by the Leakage Factor models for present-day stresses, the geometrically complex surfaces of NE-SW faults likely result in varied orientations of fluid flow along the basement fault zone, which still comprises the region where Leakage Factors are larger (Figs. 11, 12 and 15). Based on the data in this paper we postulate that the reactivated basement fault zone formed a major path for fluid and heat sourced from the lower crust and upper mantle (e.g Geissler et al., 2005.) for large periods of time, but that heat sources have now been rebalanced to result in relatively homogeneous thermal gradients (and bottom-hole temperatures) across the study area. This is an important result and shows that the recognition of fluid-flow anomalies on seismic may not correlate with enhanced thermal regimes above basement fault zones. In fact, it is the shallower Sector C that shows the higher bottom-hole temperatures and the steeper thermal gradients (Fig. 14).

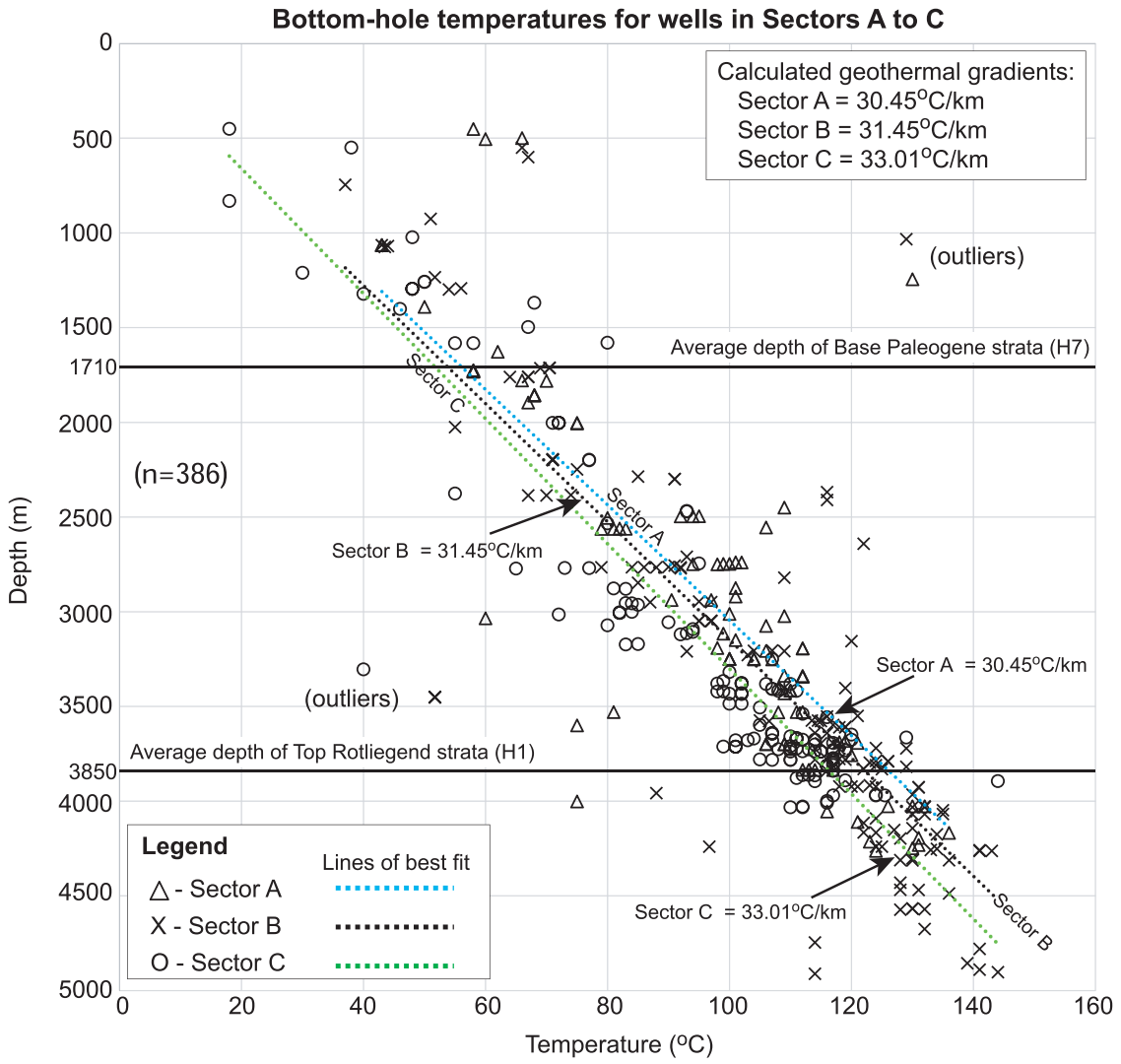

Fig. 14. Bottom-hole temperatures for key exploration wells in Sectors A to C. Thermal gradients were calculated for the three distinct sectors. A list of the wells utilised to compile this graph is shown in Supplementary File 1.

6.2. *Applicability of the proposed method to onshore geothermal prospects*

In Northern Europe, geothermal sites have mostly been found in naturally fractured reservoirs such as the Soultz-sous-Forêts and Landau sites in the Upper Rhine Graben, or the United Downs Prospect in Cornwall (Kushnir et al., 2018; Vidal and Genter, 2018; Glaas et al., 2021; Reinecker et al., 2021). These are onshore sites where heat emanates from localised, deep-rooted structures (Soultz-sous-Forêts and Landau), or result from the regional decay of radioactive elements in granitic basement rocks (United Downs). The Upper Rhine Graben records thermal anomalies along normal faults, with this heat being produced by thermal convection cells along these structures (Baillieux et al., 2013; 2014; Glaas et al., 2021). In the particular case of the Soultz-sous-Forêts site, wells have found significant geothermal heat at the base of Triassic strata, and also at the top of the Paleozoic basement, where industrial hydraulic yields of approximately 3 L/s/bar and temperatures >150 °C are able to produce electricity (3 MWe) or heat (25 MWth) (Vidal and Genter, 2018; Reinecker et al., 2021; Glaas et al., 2021). These are benchmark values considered in many a potential geothermal site in Europe.

In the Upper Rhine Graben, large basement fault zones extend through several kilometers and have significant widths. The width of the Upper Rhine Graben varies from 30 to 40 km. In the study area, the basement fault zone of interest is only 10 km wide but is part of wider region of extension within the larger Broad Fourteens Basin, itself 120 km long and 45 km wide rift basin. Paleozoic units in the Upper Rhine Graben are not similar to the study area, but basement rocks are nevertheless understood to influence regional heat flows in the Central Netherlands region. Here, tectonic models prove the existence of a heat flow pulse in Carboniferous rocks (Bonté et al., 2020). The region studied by Bonté et al. (2020) is located to the south of our study area and shows anomalous heat flow in Carboniferous strata (compared to the regional 'background' heat) resulting from the emplacement of a post-Variscan mantle plume. This mantle plume caused long-term mantle upwelling and magmatism in deep, basement rocks of a similar age and character to the study area. The reactivation history of faults in the study area, and the putative presence of basement heat sources in parts of the Netherlands (Bonté et al., 2020), suggest it to be a valid analogue to fault zones in several parts of Europe. The similarities between the study area and the Upper Rhine Graben include:

(a) Fault and fracture systems that are more pervasive near basement fault zones and, in both areas, follow the trends of orogenic events affecting the basement per se; the Rhenish and late Variscan events in the case of the Upper Rhine Graben (Glaas et al., 2021), and the Caledonian-Variscan orogeny in the study area.

(b) Fault- and fracture-related permeabilities that vary depending on

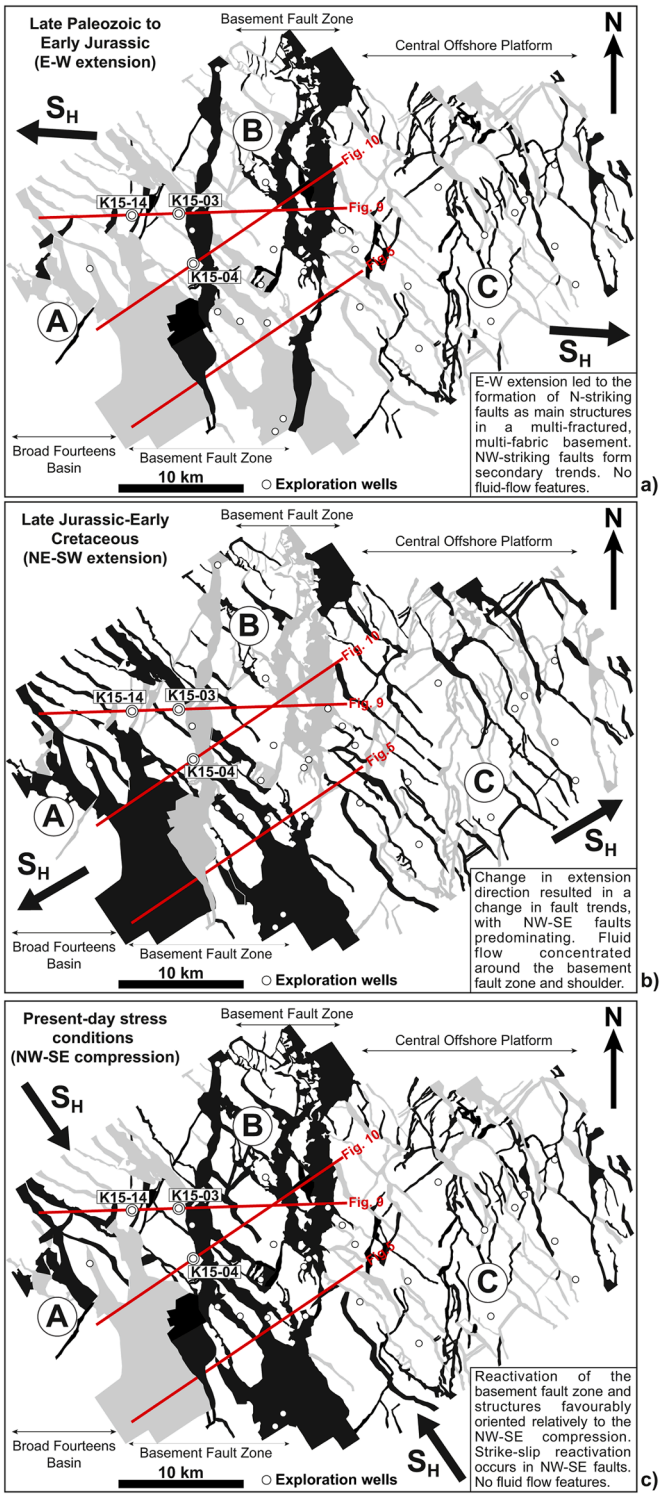

Fig. 15. Sketches illustrating the structural evolution of the study area during the main tectonic phases affecting the Southern North Sea, based on the Leakage Factor and stress analyses considered in this work. In black are shown the main basement structures reactivated during the latter tectonic phases. Grey faults are secondary structures revealing minor reactivation. The thick black arrows indicate the main directions of crustal extension and compression. (a) Triassic-Early Jurassic rifting, (b) Late Jurassic-Early Cretaceous rifting, (c) Present-day compressive stresses affecting the study area. In black are highlighted the main basement structures reactivated during the latter tectonic phases. Grey faults are secondary structures revealing minor reactivation.

their strikes, and also on the effect of present-day stress orientations (and magnitudes) on their reactivation histories. Importantly, at the sites investigated by Glaas et al. (2021) in the Upper Rhine Graben, permeable fractures are steeply dipping (85∘E and W) and strike sub-parallel to the maximum horizontal stress direction, which is extensional in nature. In this work, faults that are at an angle with the compressional NNW-SSE horizontal stresses are also prone to reactivate, forming conduits for fluid and heat.

(c) Fracture spacing distribution in the Upper Rhine Graben that is governed by power laws and negative exponential laws, with closely spaced fractures defining connected fault/fracture systems, i.e. potential fluid pathways. However, high fracture thickness and fracture density are not systematically related to high permeability. Although the vertical and horizontal resolutions of the seismic data in this paper hinder the analysis of small-scale fractures, we think the latter rule also applies to the basement fault zone of interest, as structural inheritance is an important aspect controlling the relative development (and propagation) of the faults in the study area.

A key aspect highlighted in Glaas et al. (2021) is that the most promising geothermal reservoirs in the Upper Rhine Graben (e.g. Soultz-sous-Forêts) depend on the existence of kilometre-scale hydrothermal convection cells formed between the crystalline reservoir rock and the overlying sedimentary sequences. As the convection of hot fluids in the Upper Rhine Graben can only be maintained above a threshold reservoir permeability (Guillou-Frottier et al., 2013; Magnenet et al., 2014) and requires networks of open, reservoir-scale fractures (Vidal et al., 2015; Glaas et al., 2021) it is of key importance to consider any fluid circulation between the basement fault zone in this study and the strata above the Zechstein salt. The recognition of fluid pipes and chimneys on seismic data documents the establishment of such cross-salt circulation in the past, and hints at the pervasiveness of such fluid/heat bypass zones at present (e.g., Roelofse et al., 2020.). However, in our case study, similar convection cells to the Upper Rhine Graben may not exist due to the existence of a relatively impermeable Zechstein salt above the Rotliegend strata (Figs. 9 and 10).

Laboratory studies have demonstrated that extensional fractures can increase the permeability of rock by several orders of magnitude (Morrow et al., 2001; Wang et al., 2016; Lamur et al., 2017; Pérez-Flores et al., 2017). The main reason for this enhancement has to do with the tendency of extensional stresses to open fractures that are favourably orientated (relative to local and regional stress) so that they dilate or form pull-apart jogs (e.g Peacock et al., 2002.). In contrast Kushnir et al. (2018), focusing on the smallest of fracture families in the Soultz Geothermal Site, emphasized that shear fractures in laboratory measurements may act to both increase and decrease permeability in rocks. Shear fractures in porous sandstones ($0.15 < \phi < 0.35$) were found reduce rock permeability (Zhu and Wong, 1997), whereas permeability increased with increasing inelastic strain in low porosity rocks, such as granites and volcanic rocks (Mitchell and Faulkner, 2008; Farquharson et al., 2016).

Kushnir et al. (2018) also indicated, for the Soultz-sous-Forêts site and other potential geothermal prospects, that open fracture space can influence rock permeability by following a cubic law, in which the permeability of a fracture is represented by $k_f = d^2/12$, with d representing fracture aperture (see also Pyrak-Nolte et al., 1987; Zimmerman and Bodvarsson, 1996). This cubic law considers fluid flow to be laminar and occurring between smooth, parallel plates – it is only appropriately used when fracture apertures are large or when fracture surfaces are smooth and straight. As rock fractures (and faults) are often far from reflecting ideal parallel plates (Brown, 1989), fracture tortuosity and fracture roughness will impose variations in the flow rates predicted by the cubic law above (Zimmerman et al., 1992; Zimmerman and Bodvarsson, 1996). If fractures are rough-walled, it becomes harder to determine fracture aperture, as this will vary dramatically in the 3D space (Brown, 1989; Zimmerman and Bodvarsson, 1996). Consequently, permeability values will be significantly larger than those measured in

the laboratory (Kushnir et al., 2018).

6.3. Geothermal gradients in offshore basement fault zones: Are they economically significant?

In this study, we used a 3D seismic volume to map the largest faults crossing sub-salt basement units. As with the work of Vidal and Genter (2018) we used borehole data from 38 wells to understand to what extent our case study is representative of a basement fault zone with geothermal potential, similar to other fault zones in Europe. The fault modelling undertaken in this work revealed the presence of palaeo-fluid and heat flow paths in the basement fault zone of interest (Fig. 8). Nevertheless, bottom-hole temperatures were surprisingly high, particularly for a geothermal reservoir overlain by thick salt, though they do not significantly vary within and away from the basement fault zone (Fig. 14). Assuming, as in the case of the Upper Rhine Graben, that permeability in the basement fault zone is supported by fracture and fault networks, the temperatures of 130°C-140°C recorded at borehole in the study area are within the 130°C-160°C temperature range recorded at Soultz, Landau and United Downs (Vidal and Genter, 2018; Reinecker et al., 2021; Glaas et al., 2021). We suggest the relative high temperatures documented in the study area to result from two possible reasons: a) the existence of protracted magmatic sources of heat similar to those revealed in the Central Netherlands (Blažić and Moreau, 2017; Bonté et al., 2020). In this case, the fluid pipes and chimneys imaged in the study area are not, at present, active fluid conduits – rather remnant pipes and chimneys but the heat sources that may have generated them are still active under thinned crust of the North Sea, and b) the regional cooling imposed by the Zechstein evaporites being very moderate, likely due to salt being relatively thin in the study area (Figs. 5, 9 and 10). Salt units are known to be highly conductive of heat and thus reduce the overall temperature of sedimentary basins and strata (Mello et al., 1995; McBride et al., 1999). The high bottom-hole temperatures recorded in the study area stress the limited effect salt units have on heat-flow conductivity in the Broad Fourteens Basin, at present.

We postulate that, in similarity with prospects in the Upper Rhine Graben (Landau, Insheim, Rittershoffen, Brühl, Soultz) and SW England (United Downs), basement fault zones as the one interpreted in this paper are key structures to find, and evaluate, as geothermal sites. As with the Upper Rhine Graben prospects, permeability in the study area is also associated with wide faults zones, their sub-vertical faults and fracture families.

As indicated in previous sections, no systematic differences in fault throw, length and strike are identified when crossing the basement fault zone of interest. However, contrasting with the latter observation, fluid blow-out pipes, chimneys and low-amplitude trails are still observed and interpreted on seismic data along the basement fault zone (Figs. 6, 8 and 9). These fluids were mostly sourced from the region where NW-striking syn-rift faults intersect the N-striking basement fault zone. We nonetheless consider these fluid-flow features to be relicts of past heat convention cells, or remnant gas pipes and chimneys that were left from Cretaceous time. The fact that evidence for past fluid and heat flow in the study area does not correlate with an enhanced hydrothermal system at present, stresses the importance of a detail characterisation of basement fault zones before considering them as areas with geothermal potential.

8. Conclusions

This work provides an example of a N-S basement fault zone that did not control the geometry and distribution of NW-SE faults formed around it, nor enhances heat or fluid flow at present. Nevertheless, the basement fault zone of interest was capable of focusing heat and other fluids into shallower parts of the crust during the Late Mesozoic. Any episode of tectonic reactivation - even if moderate - was likely capable of promoting the migration of large volumes of heat, lower crust volatiles such as CO_2, and gas into shallower parts of the crust. The main results of this work are summarised as follows:

(a) A basement fault zone in the Southern North Sea shows a pervasive set of NW-striking faults that were formed independently from the main basement fault zone.
(b) The incomplete strain partitioning recorded across the basement fault zone is typical of areas reactivated by regional stresses aligned with a pre-existing basement fabric. The NW-striking faults likely reflect the reactivation of an older fabric during Late Jurassic-Early Cretaceous continental rifting.
(c) The results in this work show that tectonic reactivation can lead to enhanced fluid flow along basement fault zones as the one analysed in this work.
(d) The timing and duration of such focusing of fluid and heat is an important point to consider, as the present-day temperatures show no major differences across the three sectors investigated in this work.
(e) Geothermal projects being assessed at present have equated the used of innovative methods from the oil and gas industry to accurately characterise fracture systems. Experience with 3D seismic data in multiple geothermal sites, as the one in this study, has shown promising results.

We therefore used a comprehensive data set to propose an integrated method to assess the geothermal potential of basement fault zones with the aim of allowing the extrapolation of our findings to areas where seismic and borehole data are scarcer, or poorer in quality.

Author's agreement

Dr. Tiago M. Alves put forward the idea and helped with the provision of methodology for this research as well as assessed the results of the study. Dr. Nathalia Mattos, a former PDRA at the 3D Seismic Laboratory, implemented the methodology and carried out the research. Sarah Newnes gave technical support and contributed in finalising the manuscript and its discussion. Sinéad Goodall undertook some of the fault mapping in the study area. All authors approved the final article here submitted.

Declaration of Competing Interest

The authors declare that they have no known competing financial interests or personal relationships that could have appeared to influence the work reported in this paper.

Acknowledgements

The authors would like to acknowledge the reviewers for their constructive comments. Schlumberger for the support provided to the 3D Seismic Lab. Haloil and the Joint Development Area (JDA) partners are acknowledged for the provision of seismic data on the Dutch North Sea. Borehole data are available in the NLOG website (www.nlog.nl). Editor-in-chief Christopher Bromley, A. Festa, David Bruhn and an anonymous reviewer are acknowledged for their constructive comments to an earlier version of this work. For the purpose of open access, the author has applied a Creative Commons Attribution No-derivatives (CC BY-ND) licence (where permitted by UKRI 'Open Government Licence') to any Author Accepted Manuscript version arising.

Supplementary materials

Supplementary material associated with this article can be found, in the online version, at doi:10.1016/j.geothermics.2022.102398.

References

Abramovitz, T., Thybo, H., 2000. Seismic images of Caledonian, lithosphere-scale collision structures in the southeastern North Sea along Mona Lisa Profile 2. Tectonophysics 317, 27–54. https://doi.org/10.1016/S0040-1951(99)00266-8.

Abramovitz, T., Thybo, H., the MONA LISA Working Group, 1998. Seismic structure across the Caledonian Deformation Front along MONA LISA profile 1 in the southeastern North Sea. Tectonophysics 288, 153–176. https://doi.org/10.1016/S0040-1951(97)00290-4.

Alves, T.M., Elliott, C., 2014. Fluid flow during early compartmentalisation of rafts: a North Sea analogue for divergent continental margins. Tectonophysics 634, 91–96. https://doi.org/10.1016/j.tecto.2014.07.015.

Arsenikos, S., Quinn, M., Kimbell, G., Williamson, P., Pharaoh, T., Leslie, G., Monaghan, A., 2018. Structural Development of the Devono-Carboniferous plays of the UK North Sea. Geological Society, London, Special Publications, p. 471. https://doi.org/10.1144/SP471.3 in Monaghan A.A., Underhill J.R., Hewett A.J., Marshall, J.E.v.

Bader, J.W., 2018. Structural inheritance and the role of basement anisotropies in the Laramide structural and tectonic evolution of the North American Cordilleran foreland, Wyoming. Lithosphere 11, 129–148. https://doi.org/10.1130/L1022.1.

Baillieux, P., Schill, E., Edel, J.B., Mauri, G., 2013. Localization of temperature anomalies in the Upper Rhine Graben: insights from geophysics and neotectonic activity. Int. Geol. Rev. 55 (14), 1–19. https://doi.org/10.1080/00206814.2013.794914.

Baillieux, P., Schill, E., Abdelfettah, Y., Dezayes, C., 2014. Possible natural fluid pathways from gravity pseudo-tomography in the geothermal fields of Northern Alsace (Upper Rhine Graben). Geotherm. Energy 2, 16. https://doi.org/10.1186/s40517-014-0016-y.

Ballèvre, M., Manzotti, P., Dal Piaz, G.V., 2018. Pre-Alpine (Variscan) inheritance: a key for the location of the future Valaisan Basin (Western Alps). Tectonics 37, 786–817. https://doi.org/10.1002/2017TC004633.

Bartholomew, I.D., Peters, J.M. and Powell, C.M. 1993. Regional structural evolution of the North Sea: oblique slip and the reactivation of basement lineaments. In: Geological Society, London, Petroleum Geology Conference Series, London: Geological Society of London, 4, pp. 1109–1122, 10.1144/0041109.

Bellahsen, N., Fournier, M., d'Acremont, E., Leroy, S., Daniel, J.M., 2006. Fault reactivation and rift localization: northeastern Gulf of Aden margin. Tectonics 25, TC1007. https://doi.org/10.1029/2004TC001626.

Betz, D., Führer, F., Greiner, G., Plein, E., 1987. Evolution of the lower saxony basin. Tectonophysics 137 (1–4), 127–170. https://doi.org/10.1016/0040-1951(87)90319-2.

Blažić, L., Moreau, J., 2017. Discovery of Lower Cretaceous hydrothermal vent complexes in a late rifting setting, Southern North Sea: insights from 3D imaging. J. Geol. Soc. Lond. 174 (2), 233–241. https://doi.org/10.1144/jgs2015-155.

Bonté, D., Smit, J., Fattah, R.A., Nelskamp, S., Cloething, S., van Wees, J.D., 2020. Quantifying the late-to post-Variscan pervasive heat flow, central Netherlands, Southern Permian Basin. Mar. Pet. Geol. 113, 104118 https://doi.org/10.1016/j.marpetgeo.2019.104118.

Brown, S.R., 1989. Transport of fluid and electric current through a single fracture. J. Geophys. Res. 94 (B7), 9429–9943. https://doi.org/10.1029/JB094iB07p09429.

Chopra, S., Castagna, J., Portniaguine, O., 2006. Seismic resolution and thin-bed reflectivity inversion. Can. Soc. Explor. Geophys. Rec. 31, 19–25.

Coward, M.P., Dewey, J.F., Hempton, M., Holroyd, J., Mange, M.A., 2003. Tectonic evolution. In: Evans, D., Graham, C., Armour, A., Bathurst, P. (Eds.), The Millennium Atlas: Petroleum geology of the Central and Northern North Sea. The Geological Society of London, London, pp. 17–33 editors and co-ordinators.

Daniilidis, A., Herber, R., 2017. Salt intrusions providing a new geothermal exploration target for higher energy recovery at shallower depths. Energy 118, 658–670. https://doi.org/10.1016/j.energy.2016.10.094.

Deckers, J., van der Voet, E., 2018. A review on the structural styles of deformation during late cretaceous and paleocene tectonic phases in the southern North Sea area. J. Geodyn. 115, 1–9. https://doi.org/10.1016/j.jog.2018.01.005.

Deng, C., Gawthorpe, R.L., Finch, E., Fossen, H., 2017. Influence of a pre-existing basement weakness on normal fault growth during oblique extension: insights from discree element modeling. J. Struct. Geol. 105, 44–61. https://doi.org/10.1016/j.jsg.2017.11.005.

Doornenbal, J.C., Kombrink, H., Bouroullec, R., Dalman, R.A.F., De Bruin, G., Geel, C.R., Houben, A.J.P., Jaarsma, B., Juez-Larré, J., Kortekaas, M., Mijnlieff, H.F., 2019. New insights on subsurface energy resources in the Southern North Sea Basin area. Geol. Soc. Lond. Spec. Publ. 494 https://doi.org/10.1144/SP494-2018-178. SP494-2018.

Doré, A.G., Lundin, E.R., Fichler, C., Olesen, O., 1997. Patterns of basement structure and reactivation along the NE Atlantic margin. J. Geol. Soc. Lond. 154 (1), 85–92. https://doi.org/10.1144/gsjgs.154.1.0085.

Doré, A.G., Lundin, E.R., Jensen, L.N., Birkeland, Ø., Eliassen, P.E., Fichler, C., 1999. Principal tectonic events in the evolution of the northwest European Atlantic margin. In: geological society, London, petroleum geology conference series. Geol. Soc. Lond. 5 (1), 41–61. https://doi.org/10.1144/0050041.

Dronkers, A.J. and Mrozek, F.J., 1991. Inverted basins of the Netherlands. First Break, 9 (9), 409–425, 10.3997/1365-2397.1991019.

Fazlikhani, H., Fossen, H., Gawthorpe, R.L., Faleide, J.I., and Bell, R.E., 2017. Basement structure and its influence on the structural configuration of the northern North Sea rift: Tectonics, v. 36, 10.1002/2017TC004514.

Engelder, T., 1993. Stress Regimes in the Lithosphere. Princeton University Press, Princeton, p. 486.

Farquharson, J.I., Heap, M.J., Baudm, P., 2016. Strain-induced permeability increase in volcanic rock. Geophys. Res. Lett. 43 (22), 11603–11610. https://doi.org/10.1002/2016GL071540.

Festa, A., Balestro, G., Borghi, A., De Caroli, S., Succo, A., 2020. The role of structural inheritance in continental break-up and exhumation of Alpine Tethyan mantle (Canavese Zone, Western Alps). Geosci. Front. 11, 167–188. https://doi.org/10.1016/j.gsf.2018.11.007.

Finch, E., Gawthorpe, R., 2017. Growth and Interaction of Normal Faults and Fault Network Evolution in rifts: Insights from Three-Dimensional Discrete Element Modelling. Special Publications, v, London, p. 439. https://doi.org/10.1144/SP439.23 in Childs C., Holdsworth R.E., Jackson, C.A.-L., Manzochhi, T., Walsh, J.J., and Yelding, G.: Geological Society.

Fraser, A.J., Gawthorpe, R.L., 1991. Tectono-stratigraphic development and hydrocarbon habitat of the Carboniferous of northern England. In: Hardman, R.F.P. & Brooks, J. (ed.). In: Tectonic Events Responsible for Britain's Oil and Gas Reserves, 55. Geological Society, London, Special Publication, pp. 49–86. https://doi.org/10.1144/GSL.SP.1990.055.01.03.

Fossen, H., Fazli Khani, H., Faleide, J.I., Ksienzyk, A.K., Dunlap, W.J., 2016. Post-Caledonian Extension in the West Norway–Northern North Sea region: the Role of Structural inheritance: in Childs C. Special Publications, London, p. 439. https://doi.org/10.1144/SP439.23. Holdsworth R.E., Jackson, C.A.-L., Manzochhi, T., Walsh, J.J., and Yelding, G.: Geological Societyv.

Gartman, A., Hein, J.R., 2019. Mineralization at oceanic transform faults and fracture zones. In: J. Duarte (ed.). Transform Plate Boundaries and Fracture Zones. Elsevier, pp. 105–118. https://doi.org/10.1016/B978-0-12-812064-4.00005-0.

Geissler, W., H., Kämpf, H., Kind, R., Bräuer, K., Klinge, K., Plenefisch, Th, Horálek, J., Zedník, J., and Nehybka, V., 2005. Seismic structure and location of a CO2 source in the upper mantle of the western Eger (Ohře) Rift, central Europe: Tectonics, v. 24, 10.1029/2004TC001672.

Geluk, M.C., McKie, T., Kilhams, B., 2018. An introduction to the Triassic: current insights into the regional setting and energy resource potential of NW Europe. In: Kilhams, B., Kukla, P. A., Mazur, S., Mckie, T., Mijnlieff, H. F. & Van Ojik, K. (eds). In: Mesozoic Resource Potential in the Southern Permian Basin, 469. Geological Society, London, Special Publications, pp. 139–147.

Glaas, C., Vidal, J., Genter, A., 2021. Structural characterization of naturally fractured geothermal reservoirs in the central Upper Rhine Graben. J. Struct. Geol. 148, 104370 https://doi.org/10.1016/j.jsg.2021.104370.

Gluyas, J., Mathias, S., Goudarzi, S., 2018. North Sea – next life: extending the commercial life of producing North Sea fields. In: Bowman, M., Levell, B. (Eds.), Proceedings of the Petroleum Geology of NW Europe: 50 Years of Learning 8th Petroleum Geology Conference, pp. 561–570. https://doi.org/10.1144/PGC8.30.

Gomez-Rivas, E., Martín-Martín, J.D., Bons, P.D., Griera, A., Yao, S., Llorens, M.G., Travé, A., 2019. Controls on convective fluid flow systems resulting in the formation of massive diagenetic alterations. Petrogenesis and Exploration of the Earth's Interior. Springer, Cham, pp. 223–224. https://doi.org/10.1007/978-3-030-01575-6_54.

Gondal, I.A., 2019. Offshore renewable energy resources and their potential in a green hydrogen supply chain through power-to-gas. Sustain. Energy Fuelds 3, 1468–1489. https://doi.org/10.1039/C8SE00544C.

Grollimund, B., Zoback, M.D., Wiprut, D.J., Arnesen, L., 2001. Stress orientation, pore pressure and least principal stress in the Norwegian sector of the North Sea. Pet. Geosci. 7 (2), 173–180. https://doi.org/10.1144/petgeo.7.2.173.

Guillou-Frottier, L., Carrè, C., Bourgine, B., Bouchot, V., Genter, A., 2013. Structure of hydrothermal convection in the Upper Rhine Graben as inferred from corrected temperature data and basin-scale numerical models. J. Volcanol. Geotherm. Res. 256, 29–49. https://doi.org/10.1016/j.jvolgeores.2013.02.008.

Heidbach, O., Rajabi, M., Reiter, K., Ziegler, M., and W.S.M. Team, 2016. World Stress Map Database Release 2016. GFZ Data Services, 10.5880/WSM.2016.001.

Hillis, R.R. and Nelson, E.J., 2005. January. In situ stresses in the North Sea and their applications: petroleum geomechanics from exploration to development. In Geological Society, London, Petroleum Geology Conference series, Geological Society of London, 6(1), pp. 551–564, 10.1144/0060551.

Hooker, J.N., Larson, T.E., Eakin, A., Laubach, S.E., Eichhubl, P., Fall, A., Marrett, R., 2015. Fracturing and fluid flow in a sub-décollement sandstone; or, a leak in the basement. J. Geol. Soc. Lond. 172, 428–442. https://doi.org/10.1144/jgs2014-128.

Hurter, S., Schellschmidt, R., 2002. Atlas of geothermal resources in Europe. Geothermics 32 (4–6). https://doi.org/10.1016/S0375-6505(03)00070-1, 779-78.

Jiang, F., Zhang, C., Wang, K., Zhao, Z., Zhong, K., 2019. Characteristics of micropores, pore throats and movable fluids in the tight sandstone oil reservoirs of the Yanchang Formation in the southwestern Ordos Basin, China. AAPG Bull. 103 (12), 2835–2859. https://doi.org/10.1306/03061917284.

Kim, Y.S., Sanderson, D.J., 2005. The relationship between displacement and length of faults: a review. Earth-Science Reviews 68 (3), 317–334. https://doi.org/10.1016/j.earscirev.2004.06.003.

Klein, R.J., Barr, M.V., 1986. Regional state of stress in western Europe. In: Proceedings of the ISRM International Symposium. International Society for Rock Mechanics and Rock Engineering.

Kley, J., Voigt, T., 2008. Late Cretaceous intraplate thrusting in central Europe: effect of Africa-Iberia-Europe convergence, not Alpine collision. Geology 36, 839–842. https://doi.org/10.1130/G24930A.1.

Kombrik, H., Doornenbal, J.C., Duin, E.J.T., den Dulk, M., van Gessel, S.F., ten Veen, J. H., Witmans, N., 2012. New insights into the geological structure of the Netherlands; results of a detailed mapping project. Geol. Mijnbouw 91, 419–446. https://doi.org/10.1017/S0016774600000329.

Kushnir, A.R.L., Heap, M.J., Baud, P., 2018. Assessing the role of fractures on the permeability of the Permo-Triassic sandstones at the Soultz-sous-Forêts (France) geothermal site. Geothermics 74, 181–189. https://doi.org/10.1016/j.geothermics.2018.03.009.

Lamur, A., Kendrick, J.E., Eggertsson, G.H., Wall, R.J., Ashworth, J.D., Lavallée, Y., 2017. The permeability of fractured rocks in pressurised volcanic and geothermal systems. Sci. Rep. 7, 6173. https://doi.org/10.1038/s41598-017-05460-4.

Leroy, S., Lucazeau, F., d'Acremont, E., Watremez, L., Autin, J., Rouzo, S., Bellahsen, N., Tiberi, C., Ebinger, C., Beslier, M.-O., Perrot, J., Razin, Ph., Rolandone, F., Sloan, H., Stuart, G., Al Lazki, A., Al-Toubi, K., Bache, F., Bonneville, A., Goutorbe, B., Huchon, Ph., Unternehr, P., Khanbari, K., 2010. Contrasted styles of rifting in the eastern Gulf of Aden: a combined wide-angle, multichannel seismic, and heat flow survey. Geochem. Geophys. Geosyst. 11 (7) https://doi.org/10.1029/2009GC002963.

Magnenet, V., Fond, C., Genter, A., Schmittbuhl, J., 2014. Two-dimensional THM modelling of the large scale natural hydrothermal circulation at Soultz-sous-Forêts. Geotherm. Energy 2, 17. https://doi.org/10.1186/s40517-014-0017-x.

McBride, B.C., Wiemer, P., Rowan, M.G., 1999. The effect of allochthonous salt on the petroleum systems of Northern Green Canyon and Ewing Bank (Offshore Louisiana), Northern Gulf of Mexico. Am. Assoc. Pet. Geol. Bull. 82/5B, 1083–1112.

McFarland, J.M., Morris, A.P., Ferrill, D.A., 2012. Stress inversion using slip tendency. Comput. Geosci. 41, 40–46. https://doi.org/10.1016/j.cageo.2011.08.004.

McKenna, R., D'Andrea, M., Gonzaléz, M.G., 2021. Analysing long-term opportunities for offshore energy system integration in the Danish North Sea. Adv. Appl. Energy 4, 100067. https://doi.org/10.1016/j.adapen.2021.100067.

Mello, U.T., Karner, G.D., Anderson, R.N., 1995. Role of salt in restraining the maturation of subsalt source rocks. Mar. Pet. Geol. 2 (7), 697–716. https://doi.org/10.1016/0264-8172(95)93596-V.

Michie, E.A.H., Mulrooney, M.J., Braathen, A., 2021. Fault interpretation uncertainties using seismic data, and the effects on fault seal analysis: a case study from the Horda Platform, with implications for CO_2 storage. Solid Earth 12, 1259–1286. https://doi.org/10.5194/se-12-1259-2021.

Mitchell, T.M., Faulkner, D.R., 2008. Experimental measurements of permeability evolution during triaxial compression of initially intact crystalline rocks and implications for fluid flow in fault zones. J. Geophys. Res. 113 (B11412) https://doi.org/10.1029/2008JB005588.

Moeck, I., Kwiatek, G., Zimmermann, G., 2009. Slip tendency analysis, fault reactivation potential and induced seismicity in a deep geothermal reservoir. J. Struct. Geol. 31 (10), 1174–1182. https://doi.org/10.1016/j.jsg.2009.06.012.

Morris, A., Ferrill, D.A., Henderson, D.B., 1996. Slip-tendency analysis and fault reactivation. Geology 24 (3), 275–278, 10.1130/0091-7613(1996)024<0275:STAAFR>2.3.CO;2.

Morrow, C.A., Moore, D.E., Lockner, D.A., 2001. Permeability reduction in granite under hydrothermal conditions. J. Geophys. Res. - Solid Earth 106 (B12), 30551–30560. https://doi.org/10.1029/2000jb000010.

Mulrooney, M.J., Osmond, J.L., Skurtveit, E., Faleide, J.I., Braathen, A., 2020. Structural analysis of the Smeaheia fault block, a potential CO2 storage site, northern Horda Platform, North Sea. Mar. Pet. Geol. 121, 104598 https://doi.org/10.1016/j.marpetgeo.2020.104598.

Nalpas, T., Brun, J.P., 1993. Salt flow and diapirism related to extension at crustal scale. Tectonophysics 228, 349–362. https://doi.org/10.1016/0040-1951(93)90348. N.

Nalpas, T., Le Douaran, S., Brun, J.-P., Unternehr, P., Richert, J.P., 1995. Inversion of the Broad Fourteens Basin. (Netherlands offshore), a small-scale model investigation. Sediment. Geol. 95, 237–250. https://doi.org/10.1016/0037-0738(94)00113-9.

Nielsen, L., Balling, N., Jacobsen, B.H., and MONA LISA Working Group, 2000. Seismic and gravity modelling of crustal structure in the Central Graben, North Sea. Observations along MONA LISA profile 3: Tectonophysics, 328, p. 229–244, 10.1016/S0040-1951(00)00213-4.

Omodeo-Salé, S., Eruteya, O.E., Cassola, T., Beniasad, A., Moscariello, A., 2020. Basin thermal modelling approach to mitigate geothermal energy exploration risks: the St. Gallen case study (eastern Switzerland). Geothermics 87. https://doi.org/10.1016/j.geothermics.2020.101876.

Oudmayer, B.C. and De Jager, J., 1993. January. Fault reactivation and oblique-slip in the Southern North Sea. In Geological Society, London, Petroleum Geology Conference series, Geol. Soc. Lond., 4(1), pp. 1281–1290, 10.1144/0041281.

Peacock, D., 2002. Propagation, interaction and linkage in normal fault systems. Earth-Sci. Rev. 58, 121–142. https://doi.org/10.1016/S0012-8252(01)00085-X.

Pérez-Flores, P., Wang, G., Mitchell, T.M., Meredith, P.G., Nara, Y., Sarkar, V., Cembrano, J., 2017. The effect of offset on fracture permeability of rocks from the Southern Andes Volcanic Zone, Chile. J. Struct. Geol. 104, 142–158. https://doi.org/10.1016/j.jsg.2017.09.015.

Peters, R., Vaessen, J., van der Meer, R., 2020. Offshore hydrogen production in the North Sea Enables far offshore wind development. In: Proceedings of the Offshore Technology Conference. OYC-30698-MS, Houston, Texas, USA. https://doi.org/10.4043/30698-MS, 4-7 May.

Peuchen, J., Meijninger, B.M.L., Brouwer, D., 2019. North Sea as geo database. AIMS Geosci. 5, 66–81. https://doi.org/10.3934/geosci.2019.2.66.

Pyrak-Nolte, L.J., Myer, L.R., Cook, N.G.W., Witherspoon, P.A., 1987. Hydraulic and mechanical properties of natural fractures in low permeabillity rock. In: Herget, G., Vongpaisal, S. (Eds.), Proceedings of the 6th International Congress of Rock Mechanics. Balkema Rotterdam, pp. 225–231.

Reinecker, J., Gutmanis, J., Foxford, A., Cotton, L., Dalby, C., Law, R., 2021. Geothermal exploration and reservoir modelling of the United Downs deep geothermal project, Cornwall (UK). Geothermics 97, 102226. https://doi.org/10.1016/j.geothermics.2021.102226.

Roelofse, C., Alves, T.M., Omosanya, K., 2020. Reutilisation of hydrothermal vent complexes for focused fluid flow on continental margins (Modgunn Arch, Norwegian Sea). Basin Res. 33 (2), 1111–1134. https://doi.org/10.1111/bre.12507.

Roth, F., Fleckenstein, P., 2001. Stress orientations found in northeast Germany differ from the West European trend. Terra Nova 13, 289–296. https://doi.org/10.1046/j.1365-3121.2001.00357.x.

Rowland, J.V., Sibson, R.H., 2004. Structural controls on hydrothermal flow in a segmented rift system, Taupo Volcanic Zone, New Zealand. Geofluids 4 (4), 259–283. https://doi.org/10.1111/j.1468-8123.2004.00091.x.

Scafidi, J., Wilkinson, M., Gilfillan, S.M.V., Heinemann, N., Zaszeldine, R.S., 2021. A quantitative assessment of the hydrogen storage capacity of the UK continental shelf. Int. J. Hydrog. Energy 46, 8629–8639. https://doi.org/10.1016/j.ijhydene.2020.12.106.

Scheck, M., Thybo, H., Lassen, A., Abramovitz, T., Laigle, M., 2002a. Basement Structure in the Southern North Sea, Offshore Denmark, Based On Seismic Interpretation, 201. Special Publications, London, pp. 311–326. https://doi.org/10.1144/GSL.SP.2002.201.01.15. Geological Society.

Scheck, M., Bayer, U., Otto, V., Lamarche, J., Banka, D., Pharaoh, T., 2002b. The Elbe Fault System in North Central Europe - a basement controlled zone of crustal weakness. Tectonophysics 360, 281–299. https://doi.org/10.1016/S0040-1951(02)00357-8.

Schroot, B.M., De Haan, H.B., 2003. An Improved Regional Structural Model of the Upper Carboniferous of the Cleaver Bank High based on 3D Seismic interpretation. Geological Society, 212. Special Publications, London, pp. 23–37. https://doi.org/10.1144/GSL.SP.2003.212.01.03.

Scheck-Wenderoth, M., Krzywiec, P., Maystrenko, Y., Zühlke, R., Froitzheim, N., 2008. Permian to Cretaceous tectonics of Central Europe, 2. Geological Society Special Publication, London, pp. 999–1030. https://doi.org/10.1144/CEV2P.4. In McCann, T. (Ed)Geology of Central Europe.

Selander, J., Oskin, M., Ormukov, C., Abdrakhmatov, K., 2012. Inherited strike-slip faults as an origin for basement-cored uplifts: example of the Kungey and Zailiskey ranges, northern Tian Shan. Tectonics 31. https://doi.org/10.1029/2011TC003002.

Stewart, S.A., Clark, J.A., 1999. Impact of salt on the structure of the Central North Sea hydrocarbon fairways. In: Fleet, A.J., Boldy, S.A.R. (Eds.), Proceedings of the Petroleum Geology of Northwest Europe: 5th Petroleum Geology Conference. Geological Society of London, London, pp. 179–200. https://doi.org/10.1144/0050179.

Stewart, S.A., Coward, M.P., 1995. Synthesis of salt tectonics in the southern North Sea, UK. Mar. Pet. Geol. 12 (5), 457–475. https://doi.org/10.1016/0264-8172(95)91502. G.

Sutherland, R., Townend, J., Toy, V., Upton, P., Coussens, J., Allen, M., Baratin, L.M., Barth, N., Becroft, L., Boese, C., Boles, A., 2017. Extreme hydrothermal conditions at an active plate-bounding fault. Nature 546 (7656), 137–140. https://doi.org/10.1038/nature22355.

Taillefer, A., Soliva, R., Guillou-Frottier, L., Le Goff, E., Martin, G., Seranne, M., 2017. Fault-related controls on upward hydrothermal flow: an integrated geological study of the Têt fault system, Eastern Pyrénées (France). Geofluids. https://doi.org/10.1155/2017/8190109. Article ID 8190109.

Tao, Z., Alves, T.M., 2017. The role of gravitational collapse in controlling the evolution of crestal fault systems (Espírito Santo Basin, SE Brazil) – Reply. J Struct. Geol. 98, 12–14, 0.1016/j.jsg.2017.03.005.

Tao, Z., Alves, T.M., 2019. Impacts of data sampling on the interpretation of normal fault propagation and segment linkage. Tectonophysics 762, 79–96. https://doi.org/10.1016/j.tecto.2019.03.013.

Townend, J., Sutherland, R., Toy, V.G., Doan, M.L., Célérier, B., Massiot, C., Coussens, J., Jeppson, T., Janku-Capova, L., Remaud, L., Upton, P., 2017. Petrophysical, geochemical, and hydrological evidence for extensive fracture-mediated fluid and heat transport in the Alpine Fault's hanging-wall damage zone. Geochem. Geophys. Geosyst. 18 (12), 4709–4732. https://doi.org/10.1002/2017GC007202.

Van Gent, H.W., Urai, J., De Keijzer, M., 2010. The internal geometry of salt structures – a first look using 3D seismic data from the Zechstein of the Netherlands. J. Struct. Geol. 33, 292–311. https://doi.org/10.1016/j.jsg.2010.07.005.

Van Wijhe, D.V., 1987. Structural evolution of inverted basins in the Dutch offshore. Tectonophysics 137 (1–4), 171–219. https://doi.org/10.1016/0040-1951(87)90320-9.

Verweij, J.M., Simmelink, H.J., 2002. Geodynamic and hydrodynamic evolution of the Broad Fourteens Basin (The Netherlands) in relation to its petroleum systems. Mar. Pet. Geol. 19, 339–359. https://doi.org/10.1016/S0264-8172(02)00021-1.

Verweij, J.M., Simmelink, H.J., Van Balen, R.T., David, P., 2003. History of petroleum systems in the southern part of the Broad Fourteens Basin. Netherlands J. Geosci. 82 (1), 71–90. https://doi.org/10.1017/S0016774600022800.

Verweij, J.M., Simmelink, E., Underschultz, J., 2011. Pressure and fluid flow systems in the Permian Rotliegend in the Netherlands onshore and offshore. In: Grotsch, J., Gaupp, R. (Eds.), The Permian Rotliegend of the Netherlands. SEPM Special Publication. https://doi.org/10.2110/pec.11.98.0247.

Vidal, J., Genter, A., 2018. Overview of naturally permeable fractured reservoirs in the central and southern Upper Rhine Graben: insights from geothermal well. Geothermics 74, 57–73. https://doi.org/10.1016/j.geothermics.2018.02.003.

Vidal, J., Genter, A., Schmittbuhl, J., 2015. How do permeable fractures in the Triassic sediments of Northern Alsace characterize the top of hydrothermal convective cells? Evidence from Soultz geothermal boreholes (France). Geotherm. Energy 3. https://doi.org/10.1186/s40517-015-0026-4.

Wang, L., Bayani Cardenas, M., 2016. Development of an empirical model relating permeability and specific stiffness for rough fractures from numerical deformation experiments. J. Geophys. Res. – Solid Earth, 121, 4977–4989. https://doi.org/10.1002/2016JB013004.

Wolfenden, E., Ebinger, C., Yirgu, G., Deino, A., Ayalew, D., 2004. Evolution of the northern main Ethiopian rift: birth of a triple junction. Earth Planet. Sci. Lett. 224, 213–228. https://doi.org/10.1016/j.epsl.2004.04.022.

Wu, L., Thorsen, R., Ottesen, S., Meneguolo, R., Hartvedt, K., Ringrose, P., Nazarian, B., 2021. Significance of fault seal in assessing CO_2 storage capacity and containment risks - an example from the Horda Platform, northern North Sea. Pet. Geosci. 27 https://doi.org/10.1144/petgeo2020-102 petgeo2020-102.

Ye, Q., Mei, L., Shi, H., Du, J., Deng, P., Shu, Y., Camanni, G., 2020. The influence of pre-existing basement faults on the cenozoic structure and evolution of the proximal domain, Northern South China Sea Rifted Margin. Tectonics 39. https://doi.org/10.1029/2019TC005845.

Zanella, E., Coward, M.P. and McGrandle, A., 2003. Crustal structure. The Millennium Atlas: petroleum Geology of the Central and Northern North Sea. Geological Society, London, 35, p. 43.

Zhu, W., Wong, T.F., 1997. The transition from brittle faulting to cataclastic flow: permeability evolution. J. Geophys. Res. 102 (B2), 3027–3041. https://doi.org/10.1029/96JB03282.

Ziegler, P.A., 1982. Faulting and graben formation in western and central Europe. Philos. Trans. R. Soc. London 305 (1489), 113–143. https://doi.org/10.1098/rsta.1982.0029. Series A, Mathematical and Physical Sciences.

Ziegler, P.A., 1988. Evolution of the Arctic-North Atlantic and the Western Tethys: a visual presentation of a series of Paleogeographic-Paleotectonic maps. AAPG Memoir 43, 164–196. https://doi.org/10.1306/M43478.

Ziegler, P.A., 1990. Geological Atlas of Western and Central Europe. Shell Internationale Petroleum Maatschappij B.V, 2nd ed. Distributed by the Geological Society Publishing House, Bath, p. 239. 56 encl.

Zimmerman, R.W., Bodvarsson, G.S., 1996. Hydraulic conductivity of rock fractures. Transp. Porous Media 23, 1–30. https://doi.org/10.1007/BF00145263.

Zimmerman, R.W., Chen, D.W., Cook, N.G.W., 1992. The effect of contact area on the permeability of fractures. J. Hydrol. (Amst) 139 (1–4), 79–96. https://doi.org/10.1016/0022-1694(92)90196-3.

Zoback, M.D., 2010. Reservoir geomechanics. Cambridge University Press, 461 pp, 10.1017/CBO9780511586477.

Futher reading

Quirk, D.G., 1993. Interpreting the Upper Carboniferous of the Dutch Cleaver Bank High. In: Parker, J.R. (Ed.), Proceedings of the Petroleum Geology of Northwest Europe: 4th conference. Geological Society of London, pp. 697–706.

Van der Meer, L.G.H., Kreft, E., Geel, C., Hoore, D.D., Hartman, J., 2006. Enhanced gas recovery testing in the K12-B reservoir by CO_2 injection, a reservoir engineering study. In: Proceedings of the 8th International Conference on Greenhouse Gas Control Technologies, pp. 19–22.

Van Ojik, K., Silvius, A., Kremer, Y., Shipton, Z.K., 2019. Fault seal behaviour in Permian Rotliegend reservoir sequences: case studies from the Dutch Southern North Sea. In: Ogilvie, S.R., Dee, S.J., Wilson, R.W., Bailey, W.R. (Eds.), Integrated Fault Seal Analysis. Special Publications, London, p. 496. https://doi.org/10.1144/SP496-2018-189. Geological Society.